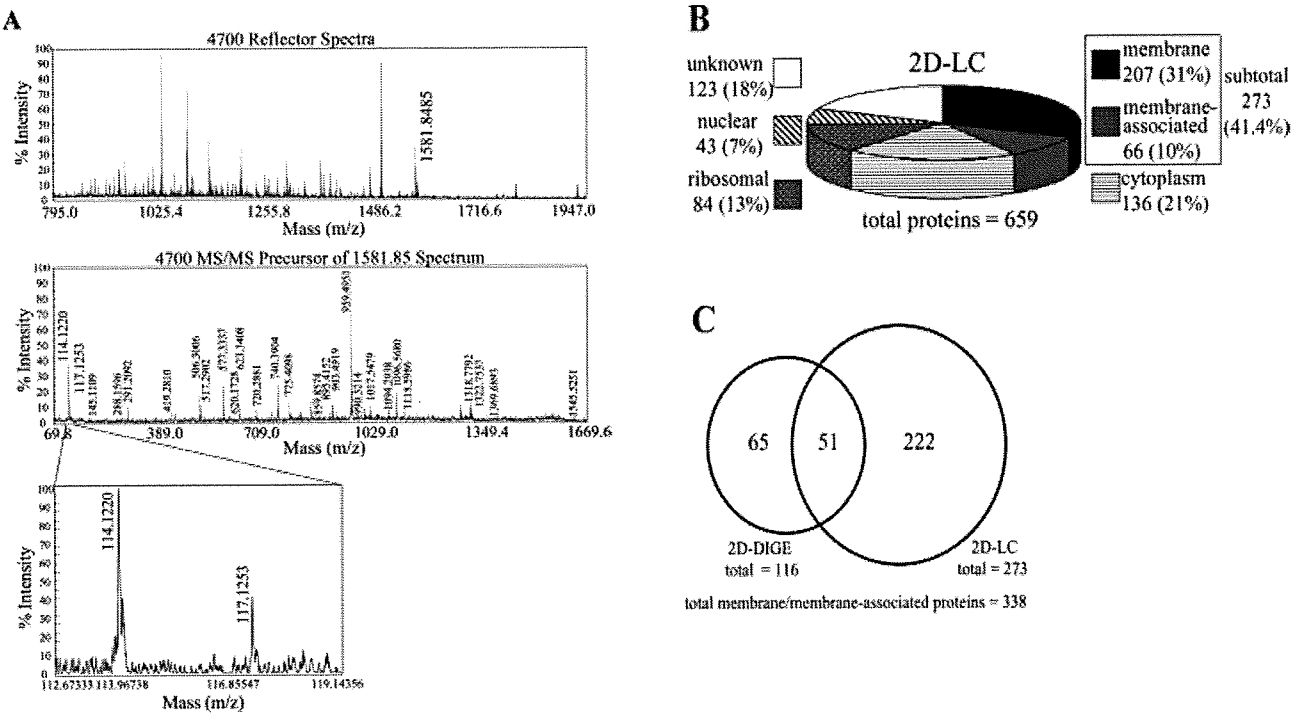

Figure 4. Shotgun-based analysis of membrane proteins of pluripotent and differentiated murine ESCs. (A) Examples of the MS and MS/MS spectra data obtained in the present study. The reporter peaks of *m/z* = 114 and 117 are from the iTRAQ reagents. The integration of the peak area reflects the quantity of peptide. (B) Subcellular localization of proteins identified using 2-D LC methods. (C) Venn diagram of shared and unique membrane and membrane-associated proteins identified by 2-D DIGE and 2-D LC. The numbers in the diagram indicate the number of identified proteins by each method.

the expression levels of a control protein, α-tubulin, were not decreased. The densitometric measurements of these bands from three independent experiments are summarized in Fig. 5B. Some of the identified proteins, *i.e.*, Slc16a1, Akt2, and ErbB4, were down-regulated to a greater extent than the well-established undifferentiated-state marker, Nanog. Immunofluorescence staining of murine ESCs cultured for 7 days without LIF further verified that the expression of these membrane proteins was specific for undifferentiated murine ESCs (Fig. 5C). Confocal microscopy of the undifferentiated murine ESCs revealed that Slc16a1 and Bsg colocalized to the surface of the plasma membrane in pluripotent murine ESCs (Fig. 5D), suggesting the cooperative action of these proteins in ESCs.

4 Discussion

Since undifferentiated murine ESCs are sensitive to extracellular stimuli, such as growth factors and extracellular matrix components, and can differentiate into various cell lineages, transmembrane and membrane-associated proteins are suggested to play important roles in the maintenance of pluripotency. In the present study, we prepared the membrane fractions from murine ESCs cultured with or without LIF for 7 days, *i.e.*, from pluripotent and differentiated cells, respectively. The observed profiles of undifferentiated cell markers (AP, Oct-3/4, and SSEA-1) and cell morphologies confirmed the successful preparation of cells used for subsequent proteomic analyses.

For the preparation of membrane fractions, two methods were used. For the 2-D DIGE analysis, the ESC surface proteins were labeled with a minimal concentration of impermeable biotinylating reagent. The membrane fractions were separated by sucrose density gradient centrifugation, and further purified using streptavidin beads. For the shotgun method, the plasma membrane fraction was prepared by sucrose density gradient centrifugation without biotinylation. Although the former method using biotin–avidin purification seems to be theoretically more effective than the latter method for the purification of membrane proteins, the results obtained from MS analyses of the former samples revealed that the percentage of membrane and membrane-associated proteins among the total identified proteins was at most 45%, while the latter method gave a similar percentage (41%). This could be due to the difficulties associated with the separation of hydrophobic proteins by IEF and SDS-PAGE. Similar results have been reported by other researchers using this method [14].

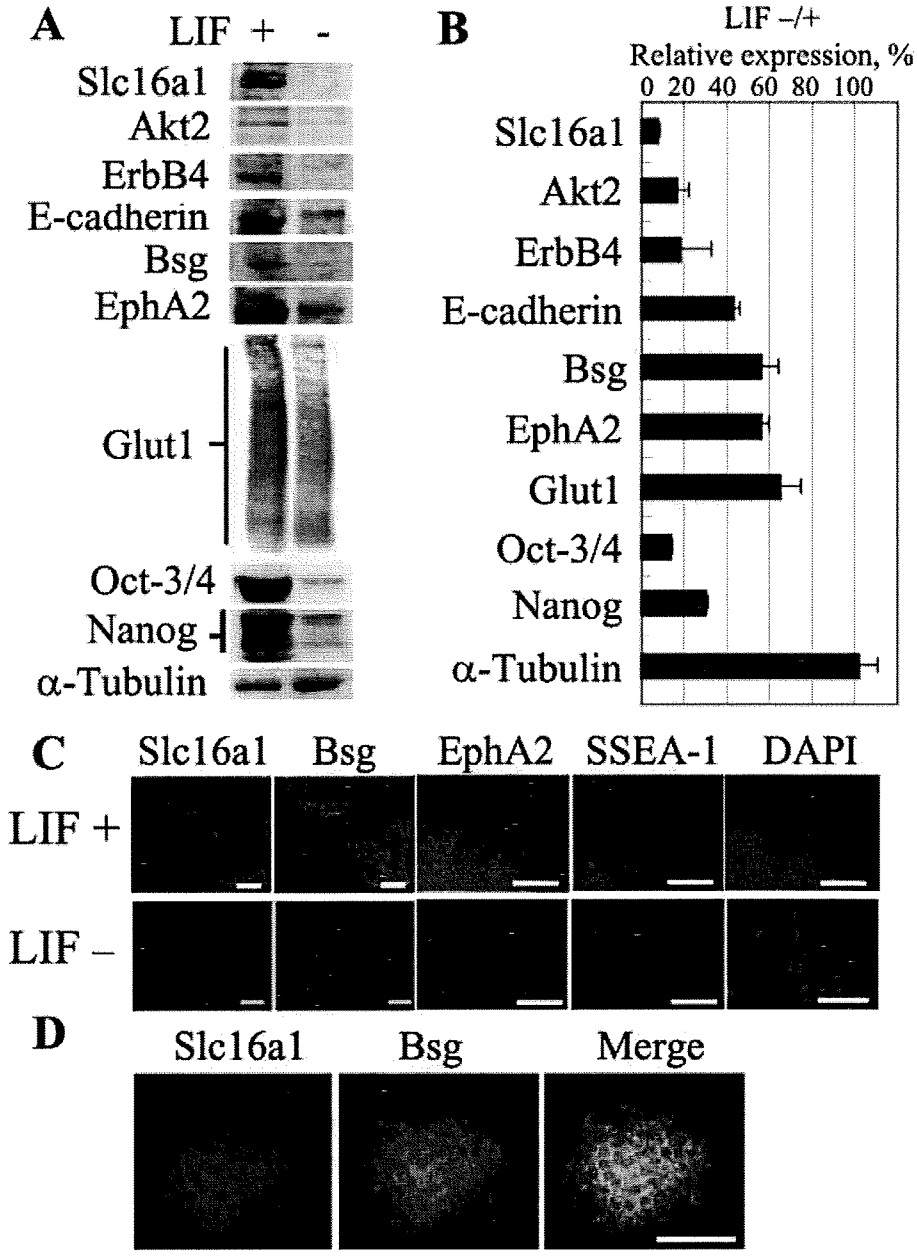

Figure 5. Undifferentiated state-specific membrane proteins expressed in murine ESCs. (A) Western blot analysis of pluripotent-specific membrane proteins in whole lysates of murine ESCs cultured for 7 days with or without LIF. The levels of these proteins were specifically decreased when the ESCs were cultured without LIF. (B) Quantification of the Western blotting in (A). The protein bands in the blots from three independent experiments were quantified using a densitometer. The amount of protein in the murine ESCs cultured with LIF was designated as 100. Error bars indicate the SEM of these experiments. The *p*-values calculated by Student's *t*-test were under 0.001. (C) Immunofluorescence analysis of the membrane proteins identified in murine ESCs. Bar, 200 μm. (D) Subcellular localization of Slc16a1 and Bsg in murine ESCs. Immunofluorescence analysis by confocal imaging reveals colocalization of Slc16a1 (red) and Bsg (green). Bar, 100 μm.

These problems can be overcome by using the shotgun method, in which membrane proteins are initially digested with a specific protease and the resultant small peptides are separated by multiple HPLCs. The shotgun method with 2-D LC gave apparently superior results to the 2-D gel-based method, and more than 80% of all the identified membrane and membrane-associated proteins were detected with this approach (Fig. 4C). Despite the disadvantage of hydrophobic membrane proteins, the 2-D gel-based method identified 33% of the total membrane and membrane-associated proteins (Fig. 4C). Moreover, the 2-D gel-based method identified 65 unique proteins that were not identified by the shotgun method. These results suggest that a complementary approach comprising the 2-D gel-based and shotgun-based methods would generate more complete lists of proteins, even when the samples were hydrophobic membrane proteins.

For the separation step of shotgun-based method, we adopted a ZIC-HILIC, with a combination of RPLC as the separation mode for the peptides after trypsin digestion. Recently, we compared this method with the most commonly used HPLC separation method, a combination of cation exchange chromatography with RPLC, using HSA as a model sample. ZIC-HILIC and RPLC gave superior separa-

Table 1. Examples of pluripotency-specific membrane proteins identified in the present study

GI accession no.	Protein identity	LIF ± ratio
gi|74183928	Solute carrier family 16 (monocarboxylic acid transporters), member 1	0.0000
gi|467233	Receptor-protein tyrosine kinase	0.1928
gi|23510249	WD repeat membrane protein PWDMP	0.2243
gi|26353502	Embigin	0.2360
gi|12836173	Solute carrier family 29 (nucleoside transporters), member 1	0.2498
gi|20072784	Thymoma viral proto-oncogene 2 (Akt2)	0.2562
gi|21730677	Chain C, alpha-catenin fragment, residues 385–651	0.2648
gi|74220144	Solute carrier organic anion transporter family, member 3a1	0.2803
gi|56748886	Sodium channel protein type 11 subunit alpha	0.2809
gi|13905180	Pyrroline-5-carboxylate reductase family, member 2	0.2901
gi|74355249	Olfactory receptor 424	0.2901
gi|94370659	Progesterone receptor membrane component 2	0.2929
gi|49750	Solute carrier family 3 (activators of dibasic and neutral amino acid transport) member 2	0.2932
gi|74215107	Solute carrier family 2 (facilitated glucose transporter), member 1	0.2963
gi|16307446	Bsg protein	0.3005
gi|11596855	Transferrin receptor	0.3105
gi|18044806	Glycoprotein, synaptic 2	0.3143
gi|83745122	Catenin (cadherin associated protein), delta 1	0.3165
gi|10946684	5-Hydroxytryptamine receptor 6	0.3249
gi|74195593	Solute carrier family 38, member 4	0.3400
gi|74198177	Integrin alpha 6	0.3434
gi|74141534	Solute carrier family 16 (monocarboxylic acid transporters), member 3	0.3438
gi|20070698	Solute carrier family 7, member 5	0.3608
gi|225753	E-cadherin	0.3618
gi|13876314	Protocadherin beta 6	0.3752
gi|94377177	Receptor-type tyrosine-protein phosphatase zeta precursor	0.3884
gi|10048460	Basal cell adhesion molecule	0.3989
gi|32057721	Olfactory receptor Olfr646	0.4383
gi|26364462	Bone marrow stromal cell antigen 2	0.4742
gi|21706627	Solute carrier family 2, member 3	0.4812
gi|22129197	Olfactory receptor 133	0.4873
gi|31560574	Integrin alpha 5	0.5086
gi|74184247	V-erb-a erythroblastic leukemia viral oncogene homolog 4	0.5128
gi|45504394	Integrin beta 1 (fibronectin receptor beta)	0.5163
gi|82659759	FAT tumor suppressor homolog 4	0.5714
gi|49903953	PTK7 protein tyrosine kinase 7	0.6286
gi|16307488	Interferon induced transmembrane protein 3	0.6712

tion of the peptide mixture and resulted in more MS/MS spectra of the peptides in the subsequent proteomic analysis (A. Intoh *et al.*, unpublished data). Our preliminary data from murine ESC membrane protein samples also suggests markedly improved protein identification with a combination of ZIC-HILIC and RPLC (data not shown).

After extensive database searching, the membrane and membrane-associated proteins specifically expressed in pluripotent murine ESCs were identified. They included receptors, channels, adhesion proteins, and signaling molecules. Among these, a pluripotent ESC-specific marker, E-cadherin, was identified. E-cadherin functions as an adhesion molecule during early embryonic development [26], and is used as a cell surface marker, as are SSEA-1 and AP activity, for ESCs [27]. We also identified β-catenin (see Supporting Information Table 2), which binds to E-cadherin [26]. Deletion of E-cadherin causes the differentiation of ESCs [28], which suggests important roles for E-cadherin in the maintenance of murine ESC pluripotency. The identification of these proteins verified the reliability of our quantitative proteomics analyses.

Some novel membrane proteins that are specifically expressed in pluripotent murine ESCs were identified. Solute carrier family 16, member 1 (Slc16a1) is one of the monocarboxylic acid transporter (Mct) family members. Bsg is a member of the Ig superfamily proteins and is a key factor in mouse blastocyst implantation [29]. Bsg interacts with Slc16a1 [29]. These two transmembrane proteins were down-regulated during the differentiation of murine ESCs (Figs. 5A–C). Colocalization of these proteins in murine

ESCs was confirmed by immunofluorescence analysis (Fig. 5D). Mct and Bsg function as essential transporters for pyruvate and lactate (but not glucose) as energy sources in very early embryogenesis [30]. Specific down-regulation of Slc16a1 and Bsg during the differentiation of murine ESCs suggests that these factors are also essential for the maintenance of the undifferentiated state of murine ESCs *in vitro*. Moreover, many solute carrier family members were identified as up- or down-regulated membrane proteins, which suggests dynamic switching of metabolite preferences during the differentiation of murine ESCs *in vitro* [31].

Another undifferentiated cell-specific protein, Akt2, is a member of the Rac serine/threonine protein kinase including Akt family, which is implicated in the regulation of cell cycle progression, cell death, adhesion, migration, metabolism, and tumorigenesis [32]. Phosphoinositide 3-kinase (PI3K)/Akt signaling has been proposed as a regulatory system for ESCs, and Akt1 is involved in the maintenance of murine and human ESCs [33]. After the withdrawal of LIF, the murine ESCs showed decreased expression of Akt2, which suggests that Akt2 plays similar functions to Akt1 in the maintenance of pluripotency. In addition, PI3K/Akt activated factors downstream of other signaling pathways, *e.g.*, basic FGF and integrins [34]. Thus, multiple signaling would cooperatively regulate the pluripotency of ESCs through activation of the PI3K/Akt signaling pathway. The increased expression of Akt2 in undifferentiated murine ESCs further underlines the importance of this protein for the maintenance of ESC multipotency.

EphA2 was also identified as a membrane protein that showed decreased expression during murine ESC differentiation upon LIF withdrawal. EphA2 is a member of the Eph family of receptor tyrosine kinases. Most Eph family members are expressed in developing embryos and tumor cells. The cellular function of EphA2 has been linked to cell proliferation [35]. The inhibition of EphA2 led to failure of growth and neoangiogenesis in human and mouse tumor cells [36]. Undifferentiated murine ESC-specific expression of EphA2 suggests the possibility that EphA2 plays similar roles in the proliferation of murine ESCs. Curiously, the expression of EphA2 is regulated by E-cadherin. Membrane localization and phosphorylation of EphA2 are dependent upon E-cadherin-mediated adhesion in mammary epithelial cells [37]. Moreover, deletion of E-cadherin leads to failure of the EphA2 receptor to localize at cell–cell contact points [38]. Cooperative down-regulation of EphA2 and E-cadherin during murine ESC differentiation may contribute to the efficient dissociation of murine ESCs from the round-shaped colonies and may promote differentiation by modulating cell proliferation.

Proteomic analysis with 2-D DIGE also identified the epidermal growth factor receptor family member ErbB4 as one of the membrane proteins down-regulated during murine ESC differentiation. ErbB4 is expressed in developing and mature organs, including the heart, breast, and brain [39]. The ErbB receptors (ErbB1–4) and their ligands, neuregulins, function cooperatively for the survival and proliferation of skeletal muscle stem cells [40]. Gene-targeted inactivation of ErbB4 in mice results in mid-embryonic lethality due to failure of myocardial trabeculae development [39]. Moreover, neuregulins promote the proliferation of hippocampus-derived neural progenitor cells (NPCs) and maintain the progenitor states of NPCs *via* the ErbB-phospholipase C/protein kinase C (PLC/PKC) pathway [41]. Thus, ErbB4 appears to be an essential factor for embryogenesis and the proliferation of stem cells. Our finding of pluripotent murine ESC-specific expression of ErbB4 suggests an additional function as a factor promoting the proliferation of murine ESCs.

In conclusion, this is the first report of the quantitative proteomics of the membrane proteins in pluripotent and differentiated ESCs. We hypothesized that pluripotent stem cells have functional and specific surface membrane proteins given their sensitivity to extracellular conditions. Indeed, various receptors and cell adhesion molecules that are specifically expressed in pluripotent murine ESCs were successfully identified, suggesting that these ligand-receptor signaling activities are crucial for murine ESC pluripotency. Moreover, other pluripotency-specific membrane proteins, such as transporters and channels, were identified. These results suggest that the transport of small molecules across the plasma membrane regulates the pluripotency of murine ESCs. These membrane proteins identified in pluripotent murine ESCs may be useful as pluripotency-specific markers or surface antigens for stem cell purification. These membrane proteins may be involved not only in the maintenance of pluripotency, but also in the reprogramming of somatic cells, as described recently [42, 43], whereby a combination of ESC-specific factors reprograms embryonic and somatic fibroblasts to induce pluripotent stem (iPS) cells. Further investigations will uncover the precise roles of these identified membrane proteins in the regulation of ESCs.

We are grateful to Chizuko Takamura for excellent technical assistance with the MALDI-TOF-MS/MS analysis.

The authors have declared no conflict of interest.

5 References

[1] Evans, M. J., Kaufman, M. H., Establishment in culture of pluripotential cells from mouse embryos. *Nature* 1981, *292*, 154–156.

[2] Martin, G. R., Isolation of a pluripotent cell line from early mouse embryos cultured in medium conditioned by teratocarcinoma stem cells. *Proc. Natl. Acad. Sci. USA* 1981, *78*, 7634–7638.

[3] Bradley, A., Evans, M., Kaufman, M. H., Robertson, E., Formation of germ-line chimaeras from embryo-derived teratocarcinoma cell lines. *Nature* 1984, *309*, 255–256.

[4] Donovan, P. J., Gearhart, J., The end of the beginning for pluripotent stem cells. *Nature* 2001, *414*, 92–97.

[5] Prelle, K., Zink, N., Wolf, E., Pluripotent stem cells–model of embryonic development, tool for gene targeting, and basis of cell therapy. *Anat. Histol. Embryol.* 2002, *31*, 169–186.

[6] Smith, A. G., Heath, J. K., Donaldson, D. D., Wong, G. G. *et al.*, Inhibition of pluripotential embryonic stem cell differentiation by purified polypeptides. *Nature* 1988, *336*, 688–690.

[7] Williams, R. L., Hilton, D. J., Pease, S., Willson, T. A. *et al.*, Myeloid leukaemia inhibitory factor maintains the developmental potential of embryonic stem cells. *Nature* 1988, *336*, 684–687.

[8] Nunomura, K., Nagano, K., Itagaki, C., Taoka, M. *et al.*, Cell surface labeling and mass spectrometry reveal diversity of cell surface markers and signaling molecules expressed in undifferentiated mouse embryonic stem cells. *Mol. Cell. Proteomics* 2005, *4*, 1968–1976.

[9] Baharvand, H., Fathi, A., van Hoof, D., Salekdeh, G. H., Concise review: Trends in stem cell proteomics. *Stem Cells* 2007, *25*, 1888–1903.

[10] Yamanaka, S., Li, J., Kania, G., Elliott, S. *et al.*, Pluripotency of embryonic stem cells. *Cell Tissue Res.* 2008, *331*, 5–22.

[11] Boiani, M., Scholer, H. R., Regulatory networks in embryo-derived pluripotent stem cells. *Nat. Rev. Mol. Cell Biol.* 2005, *6*, 872–884.

[12] Wallin, E., von Heijne, G., Genome-wide analysis of integral membrane proteins from eubacterial, archaean, and eukaryotic organisms. *Protein Sci.* 1998, *7*, 1029–1038.

[13] Hopkins, A. L., Groom, C. R., The druggable genome. *Nat. Rev. Drug Discov.* 2002, *1*, 727–730.

[14] Klein, C., Garcia-Rizo, C., Bisle, B., Scheffer, B. *et al.*, The membrane proteome of *Halobacterium salinarum*. *Proteomics* 2005, *5*, 180–197.

[15] Santoni, V., Kieffer, S., Desclaux, D., Masson, F., Rabilloud, T., Membrane proteomics: Use of additive main effects with multiplicative interaction model to classify plasma membrane proteins according to their solubility and electrophoretic properties. *Electrophoresis* 2000, *21*, 3329–3344.

[16] Unlu, M., Morgan, M. E., Minden, J. S., Difference gel electrophoresis: A single gel method for detecting changes in protein extracts. *Electrophoresis* 1997, *18*, 2071–2077.

[17] Wu, C. C., Yates, J. R., III, The application of mass spectrometry to membrane proteomics. *Nat. Biotechnol.* 2003, *21*, 262–267.

[18] Nagele, E., Vollmer, M., Horth, P., Vad, C., 2D-LC/MS techniques for the identification of proteins in highly complex mixtures. *Expert Rev. Proteomics* 2004, *1*, 37–46.

[19] Wu, W. W., Wang, G., Baek, S. J., Shen, R. F., Comparative study of three proteomic quantitative methods, DIGE, cICAT, and iTRAQ, using 2D gel- or LC-MALDI TOF/TOF. *J. Proteome Res.* 2006, *5*, 651–658.

[20] Ross, P. L., Huang, Y. N., Marchese, J. N., Williamson, B. *et al.*, Multiplexed protein quantitation in *Saccharomyces cerevisiae* using amine-reactive isobaric tagging reagents. *Mol. Cell. Proteomics* 2004, *3*, 1154–1169.

[21] Gygi, S. P., Rist, B., Gerber, S. A., Turecek, F. *et al.*, Quantitative analysis of complex protein mixtures using isotope-coded affinity tags. *Nat. Biotechnol.* 1999, *17*, 994–999.

[22] Zhao, Y., Zhang, W., White, M. A., Zhao, Y., Capillary high-performance liquid chromatography/mass spectrometric analysis of proteins from affinity-purified plasma membrane. *Anal. Chem.* 2003, *75*, 3751–3757.

[23] Iwafune, Y., Kawasaki, H., Hirano, H., Electrophoretic analysis of phosphorylation of the yeast 20S proteasome. *Electrophoresis* 2002, *23*, 329–338.

[24] Wobus, A. M., Holzhausen, H., Jakel, P., Schoneich, J., Characterization of a pluripotent stem cell line derived from a mouse embryo. *Exp. Cell Res.* 1984, *152*, 212–219.

[25] Matsui, Y., Zsebo, K., Hogan, B. L., Derivation of pluripotential embryonic stem cells from murine primordial germ cells in culture. *Cell* 1992, *70*, 841–847.

[26] Butz, S., Larue, L., Expression of catenins during mouse embryonic development and in adult tissues. *Cell Adhes. Commun.* 1995, *3*, 337–352.

[27] Viswanathan, S., Benatar, T., Rose-John, S., Lauffenburger, D. A., Zandstra, P. W., Ligand/receptor signaling threshold (LIST) model accounts for gp130-mediated embryonic stem cell self-renewal responses to LIF and HIL-6. *Stem Cells* 2002, *20*, 119–138.

[28] Larue, L., Antos, C., Butz, S., Huber, O. *et al.*, A role for cadherins in tissue formation. *Development* 1996, *122*, 3185–3194.

[29] Iacono, K. T., Brown, A. L., Greene, M. I., Saouaf, S. J., CD147 immunoglobulin superfamily receptor function and role in pathology. *Exp. Mol. Pathol.* 2007, *83*, 283–295.

[30] Herubel, F., El Mouatassim, S., Guerin, P., Frydman, R., Menezo, Y., Genetic expression of monocarboxylate transporters during human and murine oocyte maturation and early embryonic development. *Zygote* 2002, *10*, 175–181.

[31] Leese, H. J., Barton, A. M., Pyruvate and glucose uptake by mouse ova and preimplantation embryos. *J. Reprod. Fertil.* 1984, *72*, 9–13.

[32] Brazil, D. P., Yang, Z. Z., Hemmings, B. A., Advances in protein kinase B signalling: AKTion on multiple fronts. *Trends Biochem. Sci.* 2004, *29*, 233–242.

[33] Dreesen, O., Brivanlou, A. H., Signaling pathways in cancer and embryonic stem cells. *Stem Cell Rev.* 2007, *3*, 7–17.

[34] Xu, R. H., Peck, R. M., Li, D. S., Feng, X. *et al.*, Basic FGF and suppression of BMP signaling sustain undifferentiated proliferation of human ES cells. *Nat. Methods* 2005, *2*, 185–190.

[35] Fang, W. B., Brantley-Sieders, D. M., Parker, M. A., Reith, A. D., Chen, J., A kinase-dependent role for EphA2 receptor in promoting tumor growth and metastasis. *Oncogene* 2005, *24*, 7859–7868.

[36] Vearing, C. J., Lackmann, M., "Eph receptor signalling; dimerisation just isn't enough". *Growth Factors* 2005, *23*, 67–76.

[37] Zantek, N. D., Azimi, M., Fedor-Chaiken, M., Wang, B. *et al.*, E-cadherin regulates the function of the EphA2 receptor tyrosine kinase. *Cell Growth Differ.* 1999, *10*, 629–638.

[38] Orsulic, S., Kemler, R., Expression of Eph receptors and ephrins is differentially regulated by E-cadherin. *J. Cell Sci.* 2000, *113*, 1793–1802.

[39] Jones, F. E., Golding, J. P., Gassmann, M., ErbB4 signaling during breast and neural development: Novel genetic models reveal unique ErbB4 activities. *Cell Cycle* 2003, *2*, 555–559.

[40] Golding, J. P., Calderbank, E., Partridge, T. A., Beauchamp, J. R., Skeletal muscle stem cells express anti-apoptotic ErbB receptors during activation from quiescence. *Exp. Cell Res.* 2007, *313*, 341–356.

[41] Edwards, J. M., Bottenstein, J. E., Neuregulin 1 growth factors regulate proliferation but not apoptosis of a CNS neuronal progenitor cell line. *Brain Res.* 2006, *1108*, 63–75.

[42] Takahashi, K., Yamanaka, S., Induction of pluripotent stem cells from mouse embryonic and adult fibroblast cultures by defined factors. *Cell* 2006, *126*, 663–676.

[43] Takahashi, K., Tanabe, K., Ohnuki, M., Narita, M. *et al.*, Induction of pluripotent stem cells from adult human fibroblasts by defined factors. *Cell* 2007, *131*, 861–872.

Journal of Bioscience and Bioengineering
VOL. 107 No. 1, 95–97, 2009

ELSEVIER

www.elsevier.com/locate/jbiosc

TECHNICAL NOTE

Mutagenesis of longer inserts by the ligation of two PCR fragments amplified with a mutation primer

Yu Kato, Noriaki Arakawa, Yusuke Masuishi, Hiroshi Kawasaki,* and Hisashi Hirano

Supramolecular Biology, International Graduate School of Arts and Sciences, Yokohama City University, Suehiro-cho 1-7-29, Tsurumi-ku, Yokohama 230-0045, Japan

Received 11 July 2008; accepted 11 September 2008

We report a method for efficient mutagenesis of DNA in large vectors without subcloning. Two segments of the target DNA sequence, one having a mutation introduced via a mutant primer, were amplified by PCR and then the purified fragments were ligated to a vector. The mutation efficiency was nearly 100%.

[**Key words:** Polymerase chain reaction (PCR); Mutagenesis; Yeast; Expression vector; Deletion; Insertion; Substitution]

Techniques for site-directed mutagenesis have been widely used to analyze the function and regulation of genes (1–3) and the various PCR-based mutagenetic methods have improved each year (4). Among them, inverse PCR-based mutagenesis using tools such as the QuikChange® Site-Directed Mutagenesis Kit (Stratagene, La Jolla, CA, USA) is widely used (5, 6). Although this method is relatively efficient for small-size vectors (up to approximately 4000 bp), the efficiency greatly decreases as the target size increases. Additionally, for efficient mutation, the necessary length of the two complementary synthetic primers is 30–45 mer (usually longer than 40 mer). Another choice is the megaprimer method (7, 8). Although this method is applicable to large-size vectors, its lower efficiency makes it necessary to subclone the PCR product and confirm its sequence. To circumvent these problems, we report a reliable method of mutagenesis of DNA in a large-size vector (Fig. 1). We applied the method of Kadowaki et al. (9) to the mutagenesis of long inserts in a large-size vector. The method introduces mutations in DNA by ligating two fragments of the target region, one of which is amplified with a mutagenic primer by PCR. Both segments are amplified with vector-derived primers outside of the multiple-cloning site, such as a T7 promoter or T7 terminator. This PCR design makes ligation to vectors at similar cloning sites possible following digestion with restriction enzymes. Since this method amplifies only the inserts by PCR, unlike inverse PCR, mutagenesis of the targets cloned in a large-size vector such as expression vectors for yeast cells. PCR reaction used in the method is the same as routine amplification, which reduces unexpected errors. By replacing *Taq* polymerase with a high fidelity thermostable DNA polymerase with proofreading, more reliable amplification for the longer fragments to mutagenesis became possible without blunt-end treatment. The PCR products amplified by the DNA polymerase with 3′ to 5′ exonuclease activity are blunt-ended, which enables the ligation of two PCR segments without the insertion or deletion of bases, after restriction enzyme digestion at vector derived sites. Each of two purified PCR segments is successively ligated to a vector in one tube. This simple method is applicable to an insert in a large-size plasmid (e.g., cell line/yeast expression vectors) with relatively short primers (about a 20-mer). Primer design for mutagenesis is as simple as conventional PCR amplification. The PCR products could be cloned directly in the relatively large plasmid, such as pGL3-basic (4818 bp, Promega, Madison, WI, USA) and pRS425 (6849 bp, (10)), without subcloning (Table 1).

The detailed procedures to make an *MluI* cleavable site (5′-ACGCGT-3′) just downstream of the start codon of yeast *BUD8* (11) are as follows: the plasmid pYC14 (cloned with pRS425 vector, total size of 9987 bp), carrying upstream 808 bp, an open reading frame of *BUD8*, and downstream 517 bp, was used to insert an *MluI* restriction site (5′-ACGCGT-3′) just downstream of the start codon of the open reading frame. PCR was performed in two separate tubes using the corresponding sets of primer pairs, T7 promoter forward primer, 5′-TAATA CGACT CACTA TAGGG-3′ (20-mer)/BUD8_R 5′-CATAC TTCAT GTAGA ATCG-3′ (19-mer) or BUD8_F 5′-**ACGCG T** (*MluI*) ATAC AATCA GACGA AG-3′ (22-mer)/M13 reverse primer 5′-CAGGA AACAG CTATG AC-3′ (17-mer). The 50-μL reaction mixture contained 10× KOD-plus-buffer, 0.2 mM dNTP, 1 mM $MgSO_4$, 1–2 ng of the template plasmid (pYC14), 2 μM of each primer, and 1 unit of the proof-reading thermostable DNA polymerase, KOD-plus-DNA polymerase (Toyobo, Osaka). The mixture was initially run at 96 °C for 2 min, and then for 30 cycles of PCR. Each cycle consisted of denaturation at 94 °C for 15 s, annealing at 55 °C for 15 s, and extension at 68 °C for 2.5 min. The last extension step was performed at 68 °C for 7 min. After agarose-gel purification of the PCR products, one PCR fragment was digested with SpeI to remove 43 bp fragments at upstream end and the other with

* Corresponding author. Tel.: +81 045 508 7556; fax: +81 045 508 7667.
E-mail address: kawasaki@yokohama-cu.ac.jp (H. Kawasaki).

1389-1723/$ - see front matter © 2008, The Society for Biotechnology, Japan. All rights reserved.
doi:10.1016/j.jbiosc.2008.09.003

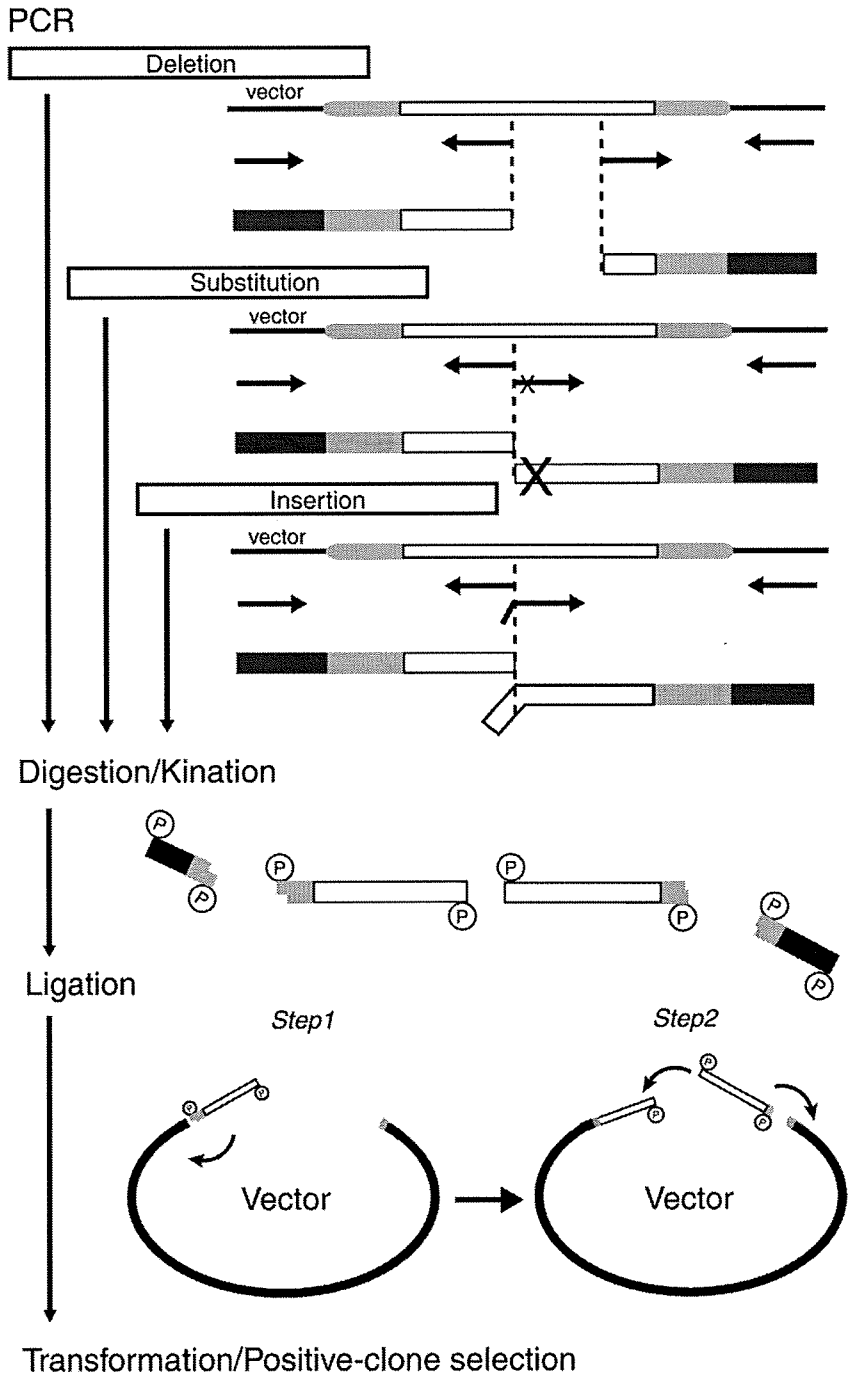

FIG. 1. Schematic illustration of the procedures used for insertion, substitution, and deletion. The forward primer for one segment and reverse primer for the other segment were vector-derived (T7 promoter and T7 terminator). The mutation was added in the specific primer to the gene of interest (GOI). Any plasmid in which the GOI was inserted could be used as a template. The black, gray, and white boxes show the backbone, multiple-cloning site, and GOI, respectively. The terminus of the PCR product near the mutation is blunt and phosphorylated, whereas the other terminus has an overhang digested with a restriction enzyme, which makes ligation to multiple vector cloning sites possible. One fragment and the predigested vector were ligated with a ligation mix for a short period, and then the other fragment was added to the same tube. The mutation was confirmed by colony PCR, restriction enzyme mapping, and sequence analysis.

*Xho*I to remove 101 bp fragments at downstream end, and the fragments were simultaneously phosphorylated with T4 polynucleotide kinase (Takara Bio, Otsu, Japan). The resulting *Spe*I and *Xho*I fragments were then purified with the Wizard® SV Gel and PCR Clean-Up System (Promega), which can remove fragments of less than 100 bp. The fragments were recovered in 20 μL of DNase-free water. The ligation of the fragments to the vector was performed by a two-step procedure: the 2.5 μL of SpeI fragments and *Spe*I/*Xho*I-digested pRS425 were incubated with 5.5 μL of ligation mix (Takara Bio) for 30 min at 16 °C in a tube. The 2.5 μL of *Xho*I fragments were then added to the same tube. The ligation reaction continued for 1 h at 16 °C. The vector, ligated with an insert DNA, was transformed to competent cells of *Escherichia coli*, XL10 Gold strain. Colony PCR was performed by using vector-derived primers, the T7 promoter primer, TAATA CGACT CACTA TAGGG (20-mer), and the M13-R primer, GGAAA CAGCT ATGAC CATGA (20-mer), generating approximately 3500-bp

TABLE 1

Mutagenesis	Vector[a]	Vector size (bp)	Insert size (bp)	Insert check[b,c]	Sequencing[d]
Deletion	pGL3-basic	4818	607[f]	5 (8)	5
Insertion	pRS425	6849	3138[g]	3 (48)[e]	3
	pRS426	5726	3245[h]	8 (48)[e]	8
	pRS305	5504	1698[i]	7 (10)	7
Substitution	pBluescript (SK−)	2961	2832[j]	8 (20)	7

[a] pRS425 pRS426 and pRS305, see Ref (10, 12). pBluescript (SK−) and pGL3-basic vectors were purchased from Stratagene and Promega, respectively.
[b] The number of colony carrying a vector with an insert is shown. The number of colony analyzed by colony PCR is shown in parentheses.
[c] Colony PCR was performed by following condition; the 10-μL reaction mixture contained 10× *Ex Taq* buffer, 0.2 mM dNTP, 2 μM of each primer, and 0.1 unit of *TaKaRa Ex Taq*™ DNA polymerase (Takara Bio). The mixture was initially run at 94 °C for 5 min, and then for 35 cycles of PCR. Each cycle consisted of denaturation at 94 °C for 30 s, annealing at 55 °C for 1 min, and extension at 72 °C for 4 min. The last extension step was performed at 72 °C for 7 min.
[d] Sequencing analysis of the inserts, which were positive by colony PCR, was carried out to confirm the mutation. The number of inserts with correct mutation is shown.
[e] Since we performed colony PCR to generate 3500-bp bands as a first-insert check screen, some colonies carrying the vector with insert were dropped by failed PCR reactions.
[f] *ANX4* at position 39801481–39802065 in chromosome II of *Homo sapiens* (NCBI accession no. NW_001838769.1).
[g] *BUD8* at position 4086–7223 in chromosome XII of *Saccharomyces cerevisiae* (NCBI accession no. U19102).
[h] *BUD9* at position 1778–3245 in chromosome VII of *Saccharomyces cerevisiae* (NCBI accession no. DQ 115391).
[i] *CGI121* at position 5575–7668 in chromosome XIII of *Saccharomyces cerevisiae* (NCBI accession no. Y07777).
[j] *BUD32* at position 205090–206869 in chromosome VII of *Saccharomyces cerevisiae* (NCBI accession no. NC_001145).

bands. The plasmids extracted from the colonies were digested with *SpeI*/*XhoI* to confirm whether they had the correct inserts. The plasmids were also subjected to sequence analysis. In this case, all colonies with an insert carried a plasmid with the insertion of the *MluI* restriction site. We also performed deletion experiments by using the pGL3-basic vector, and substitution experiments by using pBluescript (SK−) vector (Table 1).

The efficiency of mutagenesis by this method using various vectors and inserts is summarized in Table 1. In the case of random colony pickup, about 10–60% of colonies carried a vector with an insert. Sequence analysis of the inserts revealed that the mutation desired was successfully introduced into nearly 100% in the vector with an insert (Table 1). The efficiency of three-piece ligation is not high enough for longer inserts, so the ratio of colonies carrying an empty vector is a little high in some cases. In conclusion, this method for the large vectors is a very powerful tool for insertion, substitution, and deletions of base pairs in DNA.

References

1. **Ling, M. M. and Robinson, B. H.:** Approaches to DNA mutagenesis: an overview, Anal. Biochem., **254**, 157–178 (1997).
2. **Miyashita, M., Shugyo, M., and Nikawa, J. I.:** Mutational analysis and localization of the inositol transporters of *Saccharomyces cerevisiae*, J. Biosci. Bioeng., **96**, 291–297 (2003).
3. **Hosomi, N., Kawamura-Konishi, Y., Kawano, R., Fujii, I., and Suzuki, H.:** Site-directed mutagenesis study of the antibody 2D7 which catalyzes a reaction for insertion of Cu^{2+} into mesoporphyrin, J. Biosci. Bioeng., **99**, 222–229 (2005).
4. **Li, M. Z. and Elledge, S. J.:** Harnessing homologous recombination *in vitro* to generate recombinant DNA via SLIC, Nature, **4**, 251–256 (2007).
5. **Imai, Y., Matsushima, T., Sugimura, M., and Terada, A.:** simple and rapid method for generating a deletion by PCR, Nucleic Acids Res., **19**, 2785 (1991).
6. **Li, J., Li, C., Xiao, W., Yuan, D., Wan, G., and Ma, L.:** Site-directed mutagenesis by combination of homologous recombination and *DpnI* digestion of the plasmid template in *Escherichia coli*, Anal. Biochem., **373**, 389–391 (2008).
7. **Nabavi, S. and Nazar, R. N.:** Simplified one-tube "megaprimer" polymerase chain reaction mutagenesis, Anal. Biochem., **345**, 346–348 (2005).
8. **Chapnik, N., Sherman, H., and Froy, O.:** A one-tube site-directed mutagenesis method using PCR and primer extension., Anal, Biochem., **372**, 255–257 (2008).
9. **Kadowaki, H., Kadowaki, T., Wondisford, F. E., and Taylar, S. I.:** Use of polymerase chain reacrion catalyzed by *Taq* DNA polymerase for site-specific mutagenesis, Gene, **76**, 161–166 (1989).
10. **Christianson, T. W., Sikorski, R. S., Dante, M., Shero, J. H., and Hieter, P.:** Multifunctional yeast high-copy-number shuttle vectors, Gene, **110**, 119–122 (1992).
11. **Zahner, J. E., Harkins, H. A., and Pringle, J. R.:** Genetic analysis of the bipolar pattern of bud site selection in the yeast *Saccharomyces cerevisiae*, Mol. Cell. Biol., **16**, 1857–1870 (1996).
12. **Sikorski, R. S. and Hieter, P.:** A system of shuttle vectors and yeast host strains designed for efficient manipulation of DNA in *Saccharomyces cerevisiae*, Genetics, **122**, 19–27 (1989).

A Signaling Polypeptide Derived from an Innate Immune Adaptor Molecule Can Be Harnessed as a New Class of Vaccine Adjuvant[1]

Kouji Kobiyama,[3]* Fumihiko Takeshita,[2,3]* Ken J. Ishii,[†§] Shohei Koyama,[‡§] Taiki Aoshi,[†] Shizuo Akira,[‡§] Asako Sakaue-Sawano,[¶] Atsushi Miyawaki,[¶] Yuko Yamanaka,[‖] Hisashi Hirano,[‖] Koichi Suzuki,[#] and Kenji Okuda*

Modulation of intracellular signaling using cell-permeable polypeptides is a promising technology for future clinical applications. To develop a novel approach to activate innate immune signaling by synthetic polypeptides, we characterized several different polypeptides derived from the caspase recruitment domain (CARD) of IFN-β promoter stimulator 1, each of which localizes to a different subcellular compartment. Of particular interest was, N′-CARD, which consisted of the nuclear localization signal of histone H2B and the IFN-β promoter stimulator 1CARD and which localized to the nucleus. This polypeptide led to a strong production of type I IFNs and molecular and genetic analyses showed that nuclear DNA helicase II is critically involved in this response. N′-CARD polypeptide fused to a protein transduction domain (N′-CARD-PTD) readily transmigrated from the outside to the inside of the cell and triggered innate immune signaling. Administration of N′-CARD-PTD polypeptide elicited production of type I IFNs, maturation of bone marrow-derived dendritic cells, and promotion of vaccine immunogenicity by enhancing Ag-specific Th1-type immune responses, thereby protecting mice from lethal influenza infection and from outgrowth of transplanted tumors in vivo. Thus, our results indicate that the N′-CARD-PTD polypeptide belongs to a new class of vaccine adjuvant that directly triggers intracellular signal transduction by a distinct mechanism from those engaged by conventional vaccine adjuvants, such as TLR ligands. *The Journal of Immunology,* **2009, 182: 1593–1601.**

Accumulating evidence from basic research and from clinical studies clearly indicates that type I IFNs are key to the elimination of viral infection (1, 2), suppression of tumor progression (3, 4), and to vaccine immunogenicity (5). Type I IFNs, such as IFN-α and -β, are produced from a wide variety of cell types upon viral infection or in response to foreign nucleic acids, such as DNA and RNA (6–8). Recent research has dissected and elucidated the molecular basis of the ability of the immune system to sense a variety of nucleic acids as pathogen-associated molecular patterns (9) or to sense the presence of aberrant self-DNA under dangerous situations (10, 11). RIG-I-like helicases (RLHs)[4] mediate innate immune signaling in human cells induced by immunostimulatory RNAs, such as 5′-triphosphate RNA or dsRNA, or right-handed B-form DNA (B-DNA) (12–14). RLHs trigger cellular signaling through adaptor molecules, such as IFN-β promoter stimulator 1 (IPS-1, also known as MAVS/VISA/Cardif), TNFR-associating factor (TRAF) 3, and TRAF family member-associated NF-κB activator (TANK), thereby coordinating the activation of IκB kinase (IKK) family members, such as NF-κB essential modulator, IKK-α, IKK-β, TANK-binding kinase 1 (TBK1), and inducible IKK (IKKi). Once activated by such cytoplasmic kinases, NF-κB, IFN regulatory factor 3 (IRF3), and IRF7 transmigrate into the nucleus and act as master regulators of type I IFN-related gene promoters (15).

These signaling molecules contain distinct domains, and thereby associate with specific target molecules and modulate downstream signal transmission. IPS-1 plays a central role in this signaling pathway and its caspase recruitment domain (CARD) forms the death domain fold, which is structurally similar to domains of Fas-associated via death domain and caspase family members (16). The CARD of IPS-1 is essential for signal transmission through homotypic interactions with the CARDs of upstream RLHs (9). Mitochondrial sorting of IPS-1 is also crucial for its canonical

*Department of Molecular Biodefense Research, Yokohama City University Graduate School of Medicine, Yokohama, Japan; †Department of Molecular Protozoology and ‡Host Defense, Research Institute for Microbial Diseases, Osaka University, Suita, Japan; §World Premier International Immunology Frontier Research Center, Osaka University, Suita, Japan; ¶Laboratory for Cell Function Dynamics, Advanced Technology Development Group, Brain Science Institute, RIKEN, Wako, Japan; ‖Kihara Institute for Biological Research, Yokohama City University Graduate School of Integrated Science, Totsuka, Japan; and #Department of Bioregulation, National Institute of Infectious Diseases, Higashimurayama-shi, Japan

Received for publication July 24, 2008. Accepted for publication November 19, 2008.

The costs of publication of this article were defrayed in part by the payment of page charges. This article must therefore be hereby marked *advertisement* in accordance with 18 U.S.C. Section 1734 solely to indicate this fact.

[1] This work was supported, in part, by the Strategic Research Project of Yokohama City University (K18022 to F.T.), the Advancement of Medical Sciences from Yokohama Medical Foundation (to F.T. and K.K.), the National Institute of Biomedical Innovation (to K.O.), the Yasuda Medical Foundation (to F.T.), the Uehara Memorial Foundation (to F.T.), and a Grant-in-aid for Scientific Research (20590477 to F.T.) from the Ministry of Education, Culture, Sports, Science, and Technology of Japan.

[2] Address correspondence and reprint requests to Dr. Fumihiko Takeshita, Department of Molecular Biodefense Research, Yokohama City University Graduate School of Medicine, 3-9 Fukuura, Kanazawaku, Yokohama, Japan. E-mail address: takesita@yokohama-cu.ac.jp

[3] K.K. and F.T. contributed equally to this work.

[4] Abbreviations used in this paper: RLH, RIG-I-like helicase; B-DNA, B-form DNA; IPS-1, IFN-β promoter stimulator 1; TRAF, TNFR-associating factor; TANK, TRAF family member-associated NF-κB activator; TBK1, TANK binding kinase 1; IKK, IκB kinase; IKKi, inducible IKK; IRF3, IFN regulatory factor 3; CARD, caspase recruitment domain; N′-CARD, fusion of the NH_2-terminal nuclear localization signal of histone H2B to the IPS-1 CARD; PTD, protein transduction domain; TMD, transmembrane domain; NLS, nuclear localization signal; NDH, nuclear DNA helicase II; ODN, oligodeoxynucleotide; flu vax, influenza split-product vaccine; DC, dendritic cell; FL, full length; BM-DC, bone marrow-derived dendritic cell.

signaling because human hepatitis C virus NS3/4A protease inactivates IPS-1 by cleaving a region adjacent to the transmembrane domain (TMD), which is required for IPS-1 localization to the mitochondrial outer membrane (17).

To develop a novel approach to modulate innate immune signaling by synthetic polypeptides, we generated several different IPS-1 CARD-fusion polypeptides, each of which localizes to a different subcellular compartment. Of interest, the nuclear localization of a fusion polypeptide between the nuclear localization signal (NLS) of histone H2B and the IPS-1 CARD (hereafter referred to as N′-CARD) activated a distinct signaling pathway initiated from the nucleus and led to a strong production of type I IFN. Molecular and genetic analyses showed that nuclear DNA helicase II (NDH) is critically involved in this signaling pathway. Fusion of N′-CARD to the protein transduction domain (PTD), originally derived from the HIV Tat protein (18), facilitated transduction of N′-CARD from outside to inside the cell without loss of its original intracellular function. Finally, we demonstrate that the N′-CARD-PTD polypeptide acts as a novel vaccine adjuvant by directly triggering innate intracellular immune signaling to augment vaccine immunogenicity. Such a mechanism is distinct from TLR-mediated signaling, which is engaged in innate immune activation by conventional vaccine adjuvants, such as monophosphoryl-lipid A (an LPS derivative) and CpG oligodeoxynucleotide (ODN).

Materials and Methods

Cells and reagents

HEK293, HeLa, RAW264.7, and TC-1 cells were purchased from American Type Culture Collection and maintained in DMEM supplemented with 10% FCS and 50 μg/ml penicillin/streptomycin. Sf9 cells were maintained in Sf900 II SFM (Invitrogen). LPS was purchased from Sigma-Aldrich. CpG ODN, 5′-ATC GAC TCT CGA GCG TTC TC-3′, was synthesized by Gene Design. Mouse GM-CSF and Flt3L were purchased from PeproTech. Influenza split-product vaccine (flu vax) was prepared at The Research Foundation for Microbial Diseases of Osaka University (Kanon-ji city, Kagawa, Japan) from the purified influenza virus A/New Caledonia/20/99 strain (H1N1) by sequential treatment with ether and formalin, according to the method of Davenport et al. (19, 20).

Expression plasmids

The IPS-1 expression plasmid was described previously (21). The IPS-1 CARD, aa 1–100 of the IPS-1 ORF, was PCR-amplified. Fusion cDNAs were generated by ligating aa 1–100 and 514–540 of IPS-1 ORF (CARD-TMD), aa 1–37 of histone H2B ORF and aa 1–100 of IPS-1 ORF (N′-CARD), N′-CARD and aa 514–540 of hIPS-1 ORF (N′-CARD-TMD), and were amplified by PCR. These fragments were introduced in-frame into pFLAG CMV5b (Sigma-Aldrich) or pGEX6P-2 (GE Healthcare). GST-N′-CARD was further fused to the PTD (Tyr-Ala-Arg-Ala-Ala-Ala-Arg-Gln-Ala-Arg-Ala) and introduced into pFastBac HT-B (Invitrogen). TBK1, IKKi, NDH, and chloride channel 1A (CC1A) cDNAs were amplified by PCR using a human spleen cDNA library (Takara). These fragments were introduced in-frame into pFLAG-CMV4 (Sigma-Aldrich), pCIneo-HA, pCAGGS-Flag-m1SECFP, pCAG-His Venus, or pcDNA3-RFP. The N′-CARD T54A expression plasmid was generated by site-directed mutagenesis, as described previously (22). The sequences of the PCR products were confirmed using an ABI PRISM Genetic Analyzer (PE Applied Biosystems).

Luciferase assay

The luciferase assay was conducted as described previously (23).

Confocal microscopy

HeLa cells were transfected with CARD-YFP, CARD-TMD-YFP, N′-CARD-YFP, N′-CARD-TMD-YFP, IPS-1-YFP, YFP-IKKi, YFP-TBK1, and/or mRFP-NDH and incubated for 48 h. In some cases, the cells were treated with Hoechst 33258 (Invitrogen) and/or MitoTracker reagent (Invitrogen) at 37°C for 15 min. Alternatively, HeLa cells were treated with CARD or N′-CARD-PTD for 30 min. Cells were treated with Hoechst 33258 for 15 min before fixation and incubation with mouse anti-FLAG M2-Cy3. After washing with PBS containing 1% BSA, the cells were examined under an FV 500 confocal microscope (Olympus).

Immunoprecipitation and immunoblotting

Immunoprecipitation and immunoblotting was performed as described previously (24) using anti-FLAG M2 (Sigma-Aldrich), anti-FLAG M2-HRP (Sigma-Aldrich), anti-HA (Covance), anti-HA-HRP (Roche Diagnostics), anti-ubiquitin-HRP (Santa Cruz Biotechnology), anti-NDH (provided by J. D. Parvin, Brigham and Women's Hospital, Boston, MA), anti-p-JNK, anti-p-p38, anti-p-ERK, and anti-β-actin (Cell Signaling Technology).

RNA interference

An siRNA targeting NDH mRNA (stealth RNAi) was chemically synthesized by Invitrogen (Carlsbad, CA): sense, 5′-AUU GCU UGC AAA UCA UGA UCC UGU U-3′; antisense, 5′-AAC AGG AUC AUG AUU UGC AAG CAA U-3′. HEK293 cells (6×10^5) were transfected with 120 pmol of control or NDH siRNA using Lipofectamine RNAi MAX reagent (Invitrogen) according to the manufacturer's protocol.

Purification of recombinant polypeptides

DH10Bac competent cells (Invitrogen) were transformed with pFastBac HT-B-GST or with GST-N′-CARD-PTD to generate recombinant Bacmids. Sf9 cells were transfected with Bacmid-encoding GST or GST-N′-CARD-PTD to generate recombinant seed baculoviruses. Seventy-two hours after infection, the Sf9 cells were washed once with PBS and suspended in sonication buffer (50 mM Tris-HCl (pH 8.0), 50 mM NaCl, 1 mM EDTA, 1 mM DTT) containing 10% Triton X-100. After sonication, cell lysates were centrifuged at 15,000 rpm, at 4°C for 30 min. The supernatants were collected and dialyzed with sonication buffer. Recombinant polypeptides were purified using GSTrap (GE Healthcare) according to the manufacturer's protocol. In brief, after the column was equilibrated with 2 ml sonication buffer, the cell lysate was applied and the column then washed three times with 10 ml PBST (PBS containing 0.5% Triton X-100) and with PBS once. Recombinant polypeptide (GST or GST-N′-CARD-PTD) was eluted with sonication buffer containing 10 mM reduced glutathione and then dialyzed with PBS. Recombinant proteins (1 μg) used in all the experiments contained <20 fg endotoxins (*Limulus* J Single Test, Wako).

ELISA and RT-PCR

Bone marrow-derived dendritic cells (DCs) were generated by 5 days of culture with GM-CSF (20 ng/ml) (GM-DCs) or Flt3L (100 ng/ml) (FL-DCs). GM-DCs or FL-DCs were treated with or without 1, 3, or 10 μg/ml N′-CARD-PTD or 1 μM of CpG ODN for 24 h and the supernatants were subjected to ELISA for mouse IFN-α, IFN-β (PBL Biomedical Laboratories), or IL-12 p40 (Invitrogen). RAW264.7 cells were treated with 1 μg/ml LPS or 10 μg/ml N′-CARD-PTD for 3, 6, 12, 18, 24, and 48 h. The levels of mRNA for TNF-α, IL-6, IFN-α, IFN-β, IP-10, and β-actin were examined by RT-PCR as described previously (5, 22).

Immunization

Eight-week-old female BALB/c mice were administered s.c. with N′-CARD-PTD (5 μg), CpG ODN (5 μg), or flu vax (0.7 μg) alone, flu vax (0.7 μg) plus N′-CARD-PTD (5 μg), or flu vax (0.7 μg) plus CpG ODN (5 μg) at 0 and 10 days. Blood was drawn at 20 days and serum Ab titer was measured by ELISA as described previously (25). Alternatively, 8-wk-old female C57BL/6 mice were immunized with E7 peptide (E7, Arg-Ala-His-Tyr-Asn-Ile-Val-Thr-Phe, 3 μg), E7 plus N′-CARD-PTD (5 μg), or E7 plus CpG ODN (5 μg) at 0 and 2 wk. Splenocytes were harvested 2 wk after final immunization. The cells were incubated with 1 μg/ml E7 or NP peptide (Ala-Ser-Asn-Glu-Asn-Met-Glu-Thr-Met) for 18 h at 37°C. Total RNA was isolated and real-time PCR was performed as described previously (22).

Influenza challenge

Ten days after final immunization, mice were challenged intranasally with 2×10^4 pfu (8 LD_{50}) of influenza virus A/PR/8/34 (25). The body weights and mortality of the challenged mice were monitored for the next 14 days.

Tumor transplantation

Eight week-old C57BL/6 mice were administered subcutaneously with TC-1 (1×10^5 cells/mouse), a mouse lung carcinoma expressing E7 Ag (25). Mice were immunized with control NP peptide (3 μg), E7 (3 μg), N′-CARD-PTD (5 μg), or E7 (3 μg) plus N′-CARD-PTD (5 μg) at 3, 4, 5, 6, and 7 day after TC-1 inoculation. The sizes of local tumor mass were monitored for the next 20 days.

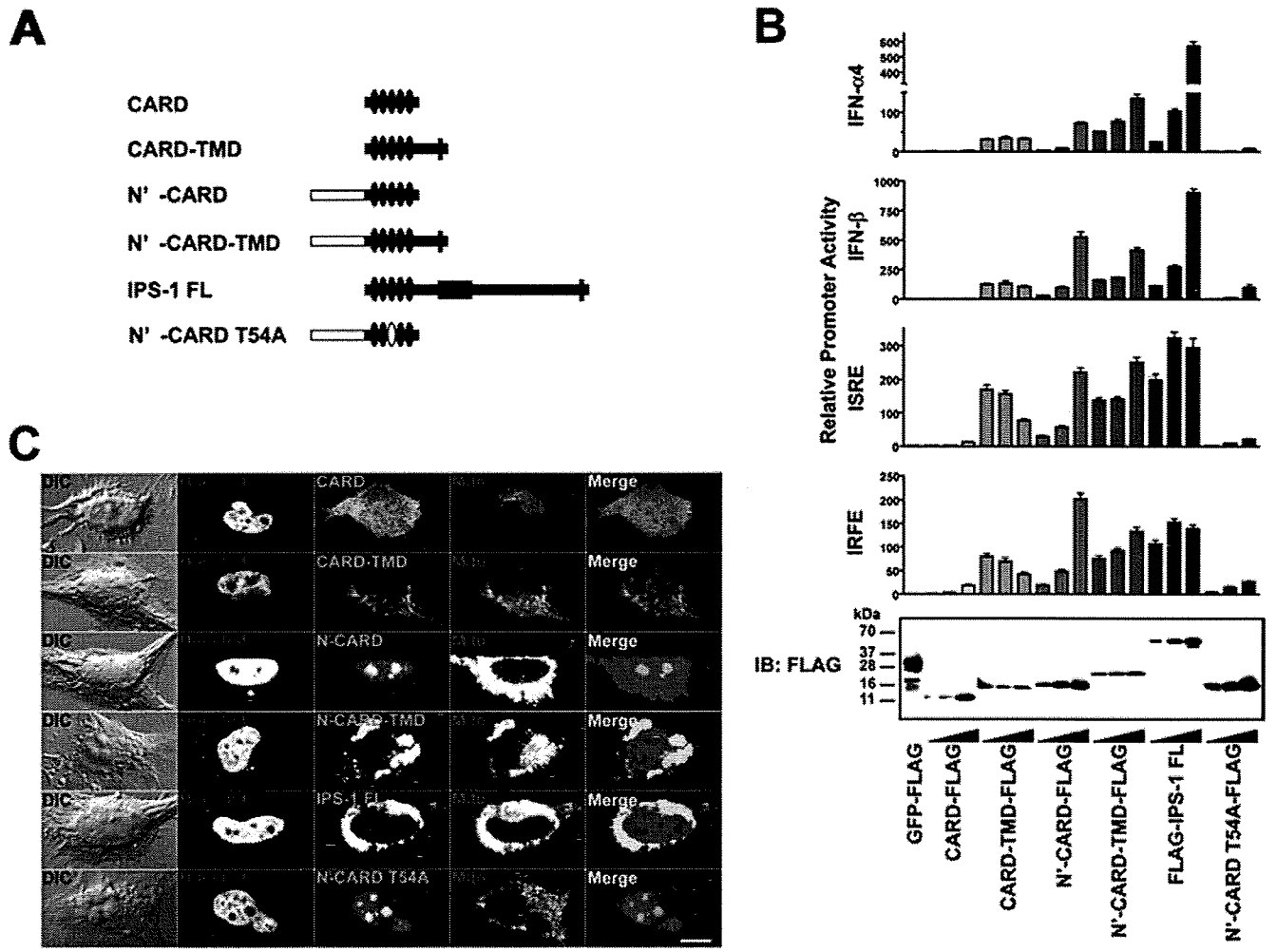

FIGURE 1. Synthetic IPS-1 CARD fusion molecules induce activation of type I IFN-related promoters. *A*, Schematic diagram of synthetic fusion molecules consisting of domains derived from IPS-1 and histone H2B. *B*, HEK293 cells were transfected with the expression plasmids, GFP-FLAG, CARD-FLAG, CARD-TMD-FLAG, N′-CARD-FLAG, N′-CARD-TMD-FLAG, FLAG-IPS-1 FL, and N′-CARD T54A-FLAG in the presence of TK-RL plus a reporter plasmid expressing firefly luciferase under the control of either the IFN-α4 promoter (*top panel*), the IFN-β promoter (*second panel from the top*), the ISRE-dependent promoter (*third panel from the top*), or the IRFE-dependent promoter (*fourth panel from the top*). Data represent means ± SD of the relative luciferase activity of six samples. Cell lysates were also subjected to immunoblot analysis to examine levels of target polypeptide expression (*bottom panel*). *C*, HeLa cells were transfected with the expression plasmids, YFP-CARD, YFP-CARD-TMD, YFP-N′-CARD, YFP-N′-CARD-TMD, YFP-IPS-1 FL, and YFP-N′-CARD T54A. Genomic DNA or mitochondria were stained with Hoechst 33258 or Mitotracker reagent, respectively, and then analyzed under a confocal microscope. The data represent one of three independent experiments with similar results. Scale bar, 10 μm.

Statistical analysis

The Student's *t* test or the Mantel-Cox log rank test was used for statistical analysis.

Results

The nuclear redistribution of IPS-1 CARD elicits type I IFN promoter activation

To elucidate the mechanisms underlying IPS-1 CARD-mediated signaling, plasmids encoding either the IPS-1 CARD alone or the IPS CARD fused to the IPS-1 TMD or to the NLS of histone H2B were generated and their abilities to induce type I IFN-related promoter activation were characterized (Fig. 1*A*). Although the CARD alone had minimal activity in eliciting such promoter activation, fusion of the TMD to the CARD (CARD-TMD) resulted in a significant activation, suggesting that the TMD facilitates CARD-mediated signaling, consistent with previous data (Fig. 1*B*; Ref. 26). Of interest, fusion of the NH_2-terminal NLS of histone H2B to the IPS-1 CARD (N′-CARD) conferred strong promoter activation, suggesting that nuclear localization of N′-CARD triggers signal activation. Indeed, N′-CARD induced phosphorylation of IRF3 at a comparable level to full length IPS-1 (FL) (Supplemental Fig. 1).[5] The mutant polypeptide N′-CARD T54A, in which the third α-helical structure of the CARD was disrupted (22), induced significantly lower levels of promoter activation, suggesting that the conformation of the IPS-1 CARD is also critical for its activity. Although N′-CARD fused to the IPS-1 TMD (N′-CARD-TMD) induced significant levels of promoter activation, the levels were comparable to those induced by N′-CARD or CARD-TMD, suggesting that the effects of CARD distribution mediated by the NLS and the IPS-1 TMD are redundant.

N′-CARD localizes to the nucleus and signals through NDH

To elucidate the signaling mechanisms triggered by N′-CARD and CARD-TMD, we examined the subcellular localizations of these fusion molecules. Confocal microscopy analysis showed that CARD-TMD fused to YFP (YFP-CARD-TMD) was present in

[5] The online version of this article contains supplemental information.

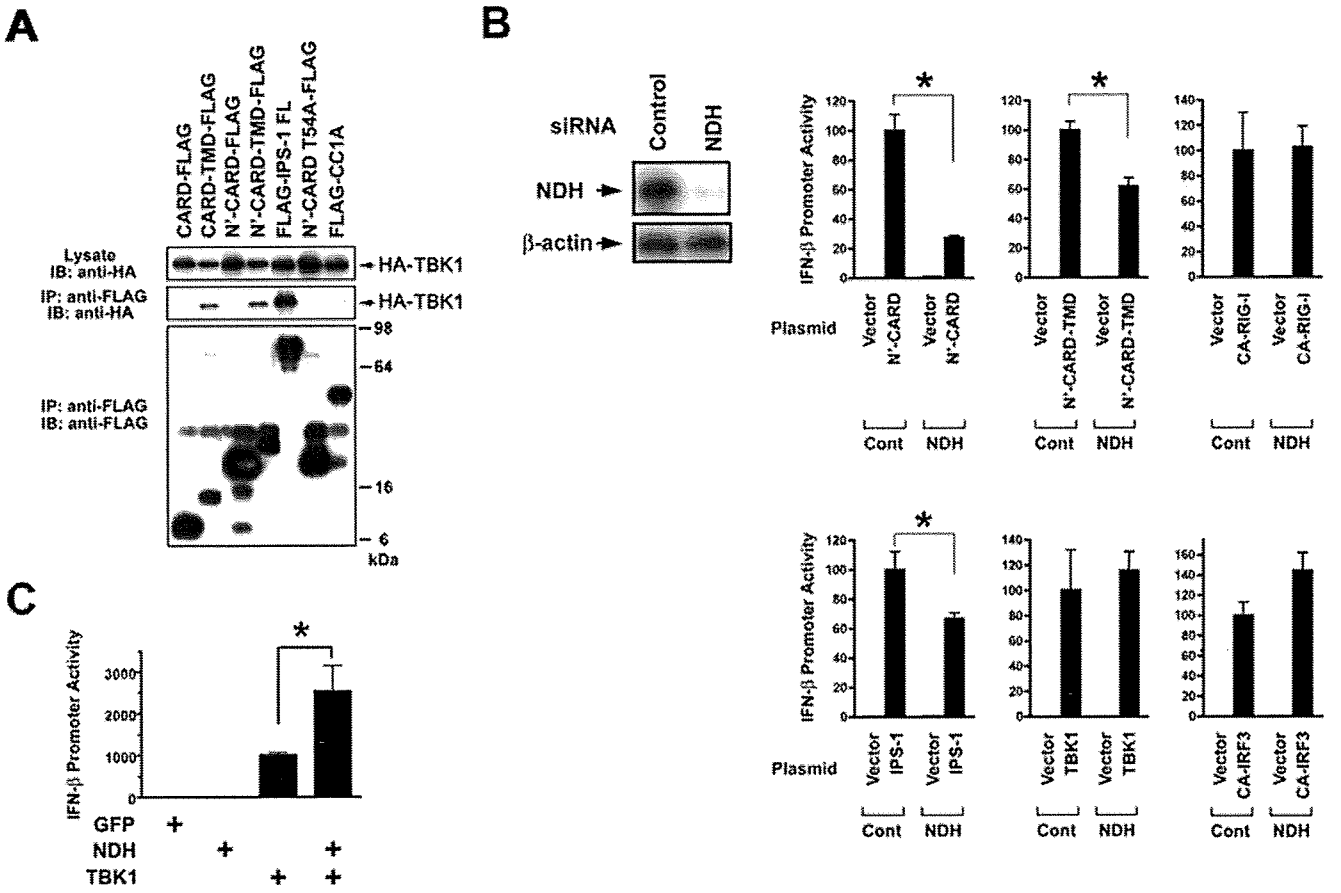

FIGURE 2. Role of NDH in N′-CARD-mediated signaling. *A*, Cell lysates from HEK293 cells transfected with the expression plasmids for HA-TBK1 plus CARD-FLAG, CARD-TMD-FLAG, N′-CARD-FLAG, N′-CARD-TMD-FLAG, FLAG-IPS-1 FL, N′-CARD T54A-FLAG, or FLAG-CC1A were prepared and immunoprecipitated with anti-FLAG Ab. The immune complexes were analyzed by immunoblotting using anti-HA or anti-FLAG Ab. *B*, After HEK293 cells were transfected with control or NDH siRNA, the levels of NDH protein were examined by immunoblotting. The cells were further transfected with the expression plasmid for N′-CARD, N′-CARD-TMD, CA-RIG-I, IPS-1, TBK1, and CA-IRF3 in the presence of TK-RL plus a reporter plasmid expressing firefly luciferase under the control of the IFN-β promoter. *C*, HEK293 cells were transfected with the expression plasmid(s) for GFP, NDH, and/or TBK1 in the presence of TK-RL plus a reporter plasmid expressing firefly luciferase under the control of the IFN-β promoter. *B* and *C*, Forty eight hours after transfection, luciferase assay was performed. Data represent means $\pm$ SD of the relative luciferase activity of eight samples. *, $p < 0.05$.

mitochondria, with a localization pattern similar to that of IPS-1 FL (YFP-IPS-1 FL), while N′-CARD fused to YFP (YFP-N′-CARD) was mostly present in the nuclear interchromosomal space (Fig. 1*C*). Because CARD alone (YFP-CARD) was present diffusely within the cell and both YFP-N′-CARD and YFP-N′-CARD T54A localized to the nucleus, it was suggested that the NLS directed the nuclear distribution of the IPS-1 CARD (Fig. 1*C*). These results implied that N′-CARD triggers cellular signaling pathways that originate in the nucleus and that are distinct from those triggered by CARD-TMD or IPS-1 FL, which originate from mitochondria.

TBK1, and its closely related IKK family member IKKi, are kinases acting downstream of IPS-1 and are required for a type I IFN production (21, 26, 27). We next examined the molecular interactions between each CARD-fusion molecule and TBK1 by immunoprecipitation analysis. As a control, TBK1 was coprecipitated with IPS-1 FL (Fig. 2*A*). A significant amount of TBK1 was also detected after precipitation with CARD-TMD or N′-CARD-TMD, but not after precipitation with CARD, N′-CARD, or N′-CARD T54A, suggesting that the TMD supports the association of the CARD with TBK1 (Fig. 2*A*).

To examine the signaling mechanisms triggered by N′-CARD, we tried to identify cellular molecules that associate with N′-CARD using a tandem-affinity purification system and TOF-MS analysis (data not shown). Among the N′-CARD interacting molecules identified, we were particularly interested in nuclear DNA helicase II (NDH, also known as RNA helicase A), a 1270 amino acid protein containing two copies of a dsRNA binding domain, a DEIH (Asp-Glu-Ile-His) helicase core, and an RGG (Arg-Gly-Gly) box nucleic acid-binding domain.

To examine the functional role of NDH in the signaling pathway leading to type I IFN production, NDH mRNA was ablated by RNA interference. Endogenous NDH protein was specifically decreased by NDH siRNA but not by control siRNA treatment (Fig. 2*B*). Knockdown of NDH resulted in a suppression of N′-CARD-induced IFN-β promoter activation by 73%. The level of promoter activation induced by IPS-1 or N′-CARD-TMD was also partially suppressed in NDH-knockdown cells by 33 and 38%, respectively. The levels were comparable when a constitutively active form of RIG-I (RIG-I 2CARDs), TBK1, or a constitutively active form of IRF3 (IRF3CA) was examined (Fig. 2*B*). Although over-expression of NDH had no effect, and over-expression of TBK-1 had a minimal effect on IFN-β promoter activation, over-expression of NDH plus TBK1 synergistically activated the IFN-β promoter, suggesting that NDH had the ability to up-regulate TBK1 activity (Fig. 2*C*). These results, taken together, suggest that NDH is involved in the events downstream of N′-CARD, and partially in

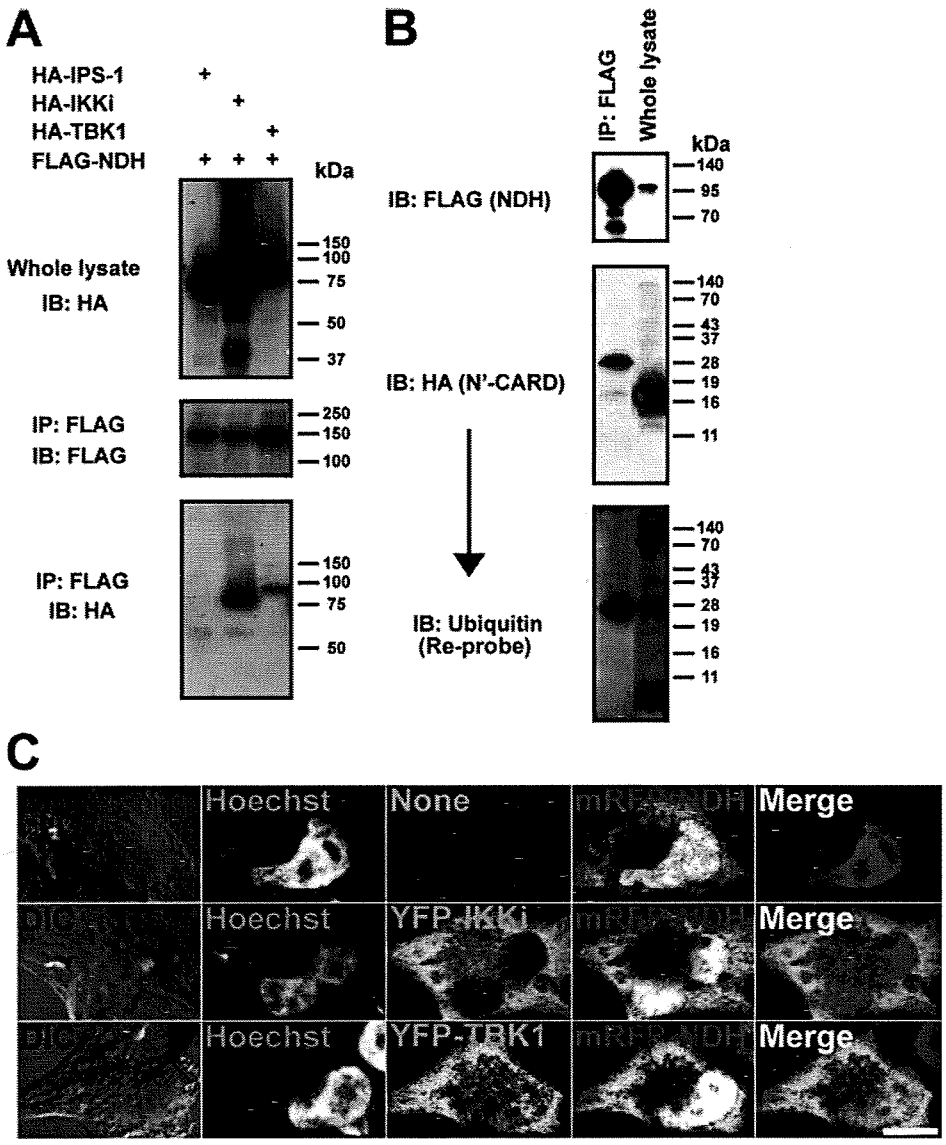

FIGURE 3. NDH associates with N′-CARD, TBK1, and IKKi. *A* and *B*, The lysates of HEK293 cells transfected with the expression plasmids for FLAG-NDH plus HA-IPS-1, HA-IKKi, HA-TBK1 (*A*) or N′-CARD-HA (*B*) were prepared and immunoprecipitated with anti-FLAG Ab. The immunoblots were probed with anti-HA or anti-FLAG Ab (*A* and *B*) or sequentially probed with anti-HA and anti-ubiquitin Ab (*B*). *C*, HeLa cells were transfected with an expression plasmid for mRFP-NDH alone or with those for mRFP-NDH and YFP-IKKi or YFP-TBK1. After staining with Hoechst 33258, the cells were examined under a confocal microscope. Data represent one of three independent experiments with similar results. Scale bar, 10 μm.

those downstream of IPS-1, and that it plays a role in signaling upstream of TBK1.

To confirm the physical interactions among NDH, IKKi, TBK1, and N′-CARD, immunoprecipitation analysis was performed. A strong interaction was detected between NDH and IKKi or TBK1, while there was no apparent association of NDH with IPS-1 in this assay (Fig. 3*A*). By contrast, NDH was confirmed to interact with N′-CARD. Of interest, the mobility of N′-CARD coprecipitated with NDH was retarded in SDS-PAGE (~25 kDa) when compared with that in whole cell lysate (~18 kDa) (Fig. 3*B*). The retarded N′-CARD was detected by anti-ubiquitin Ab, suggesting that mono-ubiquitinated N′-CARD, directly or indirectly, has the ability to associate with NDH (Fig. 3*B*). We also examined the subcellular localization of NDH, IKKi, and TBK1 by confocal microscopy analysis (Fig. 3*C*). Both YFP-IKKi and YFP-TBK1 were mostly present in the cytoplasm, while mRFP-NDH was diffusely present within the cell. Most NDH present within the cytoplasm colocalized with IKKi or TBK1 (Fig. 3*C*).

Recombinant N′-CARD polypeptide fused to the protein transduction domain (N′-CARD-PTD) induces type I IFN production and exerts innate immune responses in vitro

To examine the potent ability of N′-CARD in modulating innate immune responses, we generated a recombinant N′-CARD polypeptide fused to the PTD, which enables transduction of extracellular protein into intracellular compartments. When the N′-CARD-PTD polypeptide was added to the culture medium of HeLa cells, it entered the nucleus within 30 min (Fig. 4*A*). By contrast, when the same amount of CARD polypeptide was added, only a minimal level of the polypeptide was observed inside the cell (Fig. 4*A*). The addition of the N′-CARD-PTD polypeptide alone induced significant levels of IFN-β promoter activation in HEK293 cells, suggesting that N′-CARD-PTD has the ability to transmigrate into the cell and trigger NDH-mediated cellular signaling to elicit type I IFN production (Supplemental Fig. 2).

We next examined whether administration of the N′-CARD-PTD polypeptide activates immune cells in vitro. As shown in Fig. 4*B*, N′-CARD-PTD induced production of a proinflammatory cytokine (TNF-α), type I IFNs (IFN-α and -β), and an IFN-stimulated gene product (IP-10) in a mouse macrophage cell line, RAW264.7. The expression of IFN-α and -β mRNAs was detected within 18 h; the expression of IFN-α mRNA continued for more than 48 h after N′-CARD-PTD treatment. By contrast, LPS, an activator of TLR4-mediated innate immune responses, induced IFN-β mRNA within 3 h, but this induction lasted for less than 18 h. The overall level of IFN-α mRNA production was higher in cells stimulated with N′-CARD-PTD compared with those stimulated with LPS, while that of IFN-β was lower in those stimulated

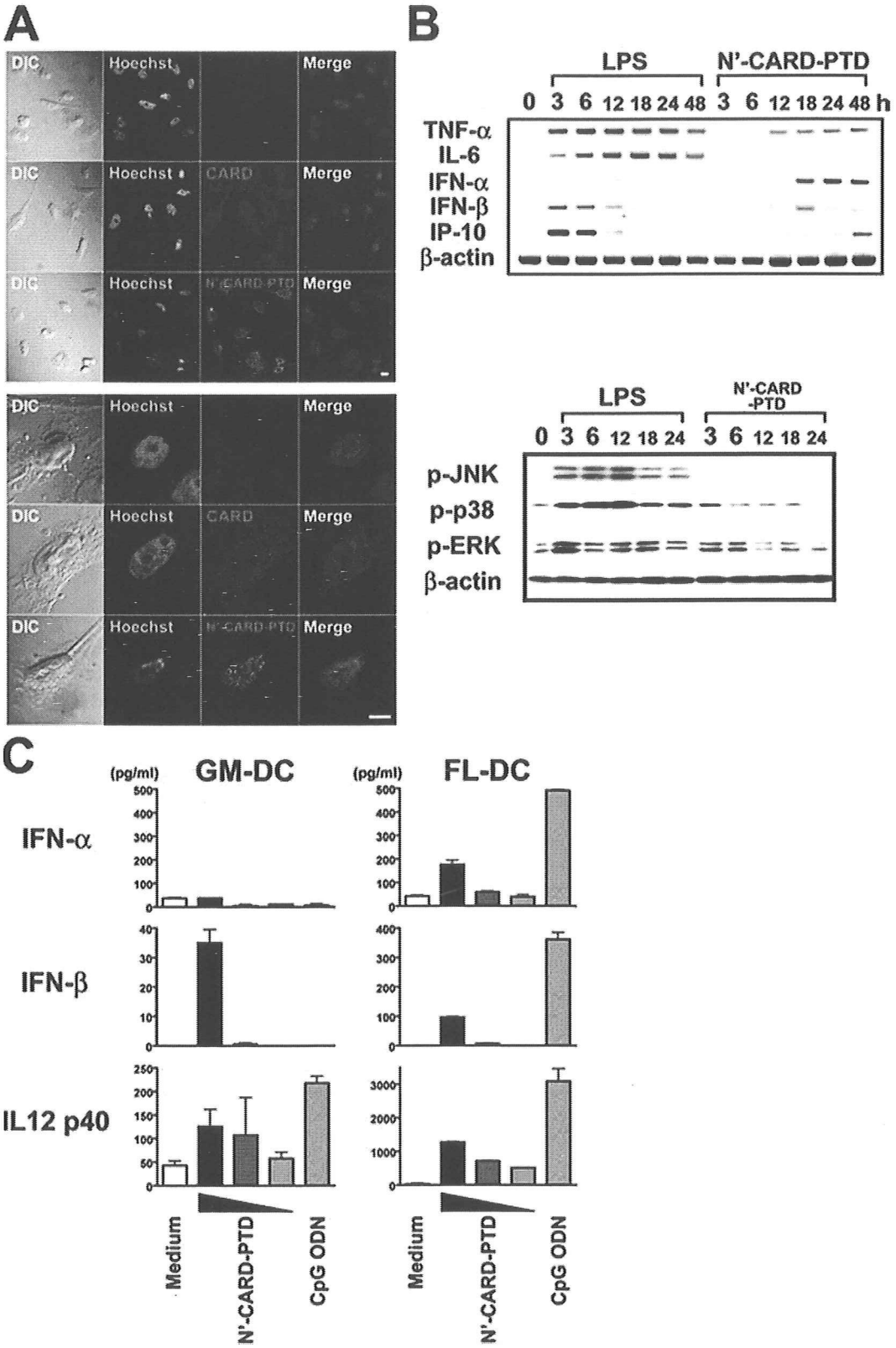

FIGURE 4. The N′-CARD-PTD polypeptide induces type I IFN production and DC maturation. *A*, Recombinant CARD or N′-CARD-PTD polypeptide was administered into the culture medium of HeLa cells. Thirty minutes after addition, the cells were permeabilized, stained with anti-FLAG M2-Cy3 and Hoechst 33258, and subjected to confocal microscopy analysis. *Upper panel,* Lower magnification. *Lower panel,* Higher magnification. Scale bar, 10 μm. *B*, RAW264.7 cells were treated with 1 μg/ml LPS or 10 μg/ml N′-CARD-PTD for 3, 6, 12, 18, 24, and 48 h. The levels of mRNA expression for TNF-α, IL-6, IFN-α, IFN-β, IP-10 and β-actin were examined by RT-PCR (*upper panel*). The levels of phosphorylated JNK, p38, or ERK were examined by immunoblotting (*lower panel*). *C*, GM-DCs or FL-DCs were treated with or without 1, 3, or 10 μg/ml N′-CARD-PTD or 1 μM of CpG ODN for 24 h and the supernatants were subjected to ELISA for mouse IFN-α, IFN-β, or IL-12 p40. Data represent one of two or three independent experiments with similar results.

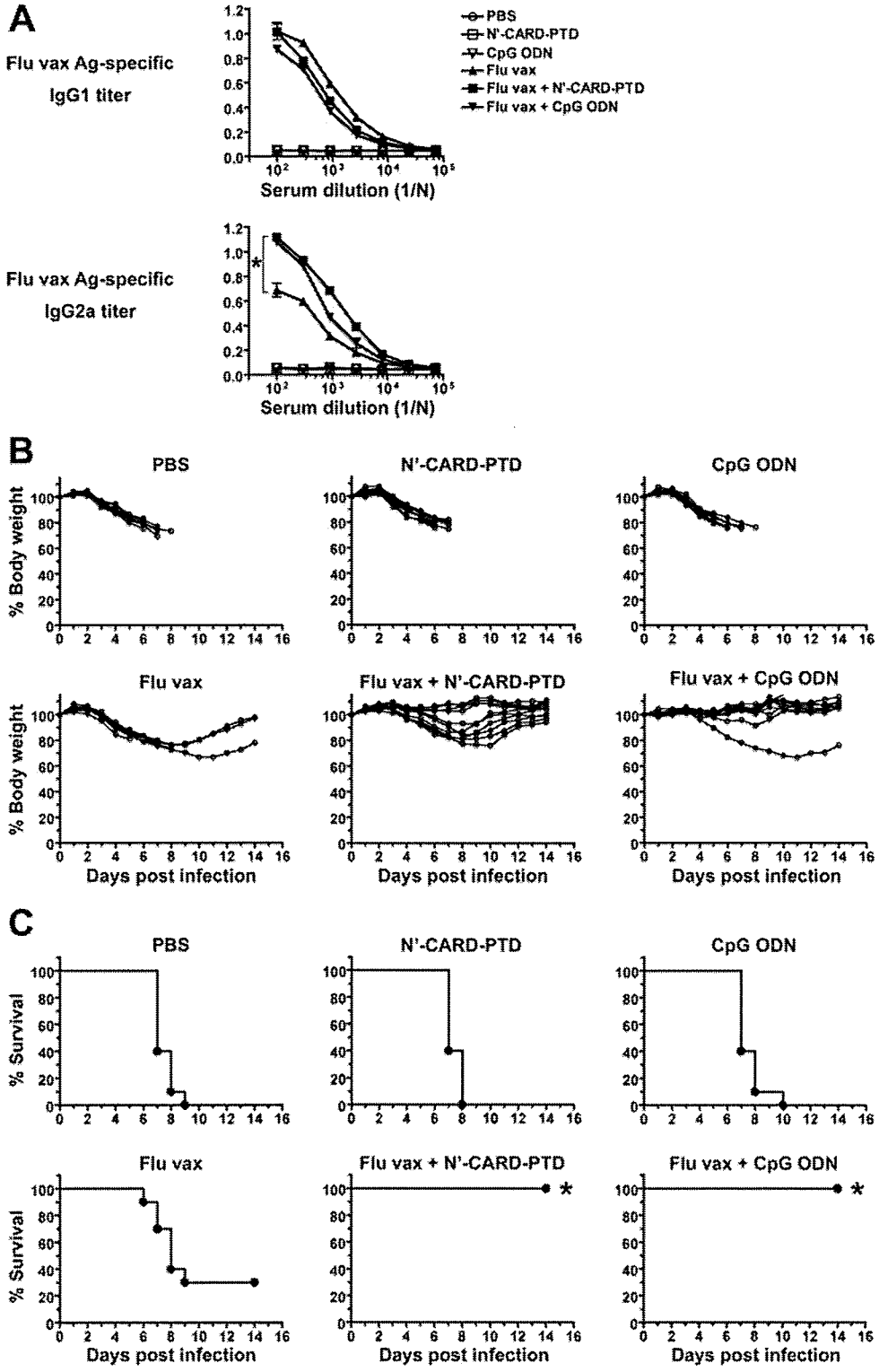

FIGURE 5. Coadministration of N′-CARD-PTD enhances Ag-specific IgG2a production and superior protection against lethal influenza infection. *A–C*, Eight-week-old female BALB/c mice (n = 10) were immunized s.c. with flu vax (0.7 μg), N′-CARD-PTD (5 μg), CpG ODN (5 μg), flu vax (0.7 μg) plus N′-CARD-PTD (5 μg), or flu vax (0.7 μg) plus CpG ODN (5 μg) at 0 and 10 days. *A*, Anti-flu vax Ab titer was examined 10 days after the final immunization. *B* and *C*, Ten days after the final immunization, mice were challenged with 8 LD_{50} doses of influenza A/P/R8 (H1N1). The bodyweight changes (*B*) and the mortality (*C*) were monitored for the next 14 days. Data represent one of two independent experiments with similar results. *, $p < 0.05$.

with N′-CARD-PTD compared with those stimulated LPS (Fig. 4*B*). These results suggest that N′-CARD-PTD activates a distinct innate immune signaling pathway(s) from those engaged by LPS. In fact, LPS induced phosphorylation of MAPK such as JNK, p38, and ERK within 3 h, while N′-CARD-PTD had little effects on activation of these kinases except for ERK at 3 and 6 h (Fig. 4*B*). We also examined whether N′-CARD-PTD activates bone marrow-derived dendritic cells (BM-DCs). As a control, CpG ODN activated BM-DCs induced in vitro by Flt3L (FL-DCs) but not BM-DCs induced in vitro by GM-CSF (GM-DCs) to produce type I IFNs. N′-CARD-PTD, by contrast, activated both GM-DCs and FL-DCs to produce type I IFNs (Fig. 4*C*). We also observed that N′-CARD-PTD weakly but significantly up-regulated cell surface expression of MHC class I, class II, CD40, and CD86 on both GM-DCs and FL-DCs (data not shown). Up-regulation of such cell surface molecules was dependent on type I IFN production but independent on myeloid differentiation factor 88 (MyD88) nor Toll-IL-1R domain-containing adaptor-inducing IFN-β (TRIF) (data not shown).

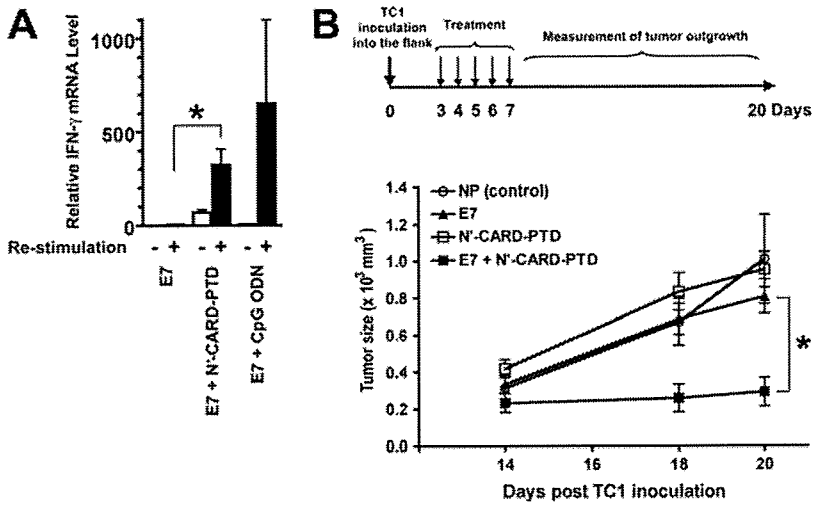

FIGURE 6. Coadministration of N′-CARD-PTD plus tumor-associated Ag E7 confers superior protection against tumor outgrowth. *A*, Eight-week-old female BALB/c mice ($n = 5$) were immunized subcutaneously with E7 peptide (3 μg), E7 peptide (3 μg) plus N′-CARD-PTD (5 μg), or E7 peptide (3 μg) plus CpG ODN (5 μg) at 2 and 4 wk. Splenocytes were prepared from each individual mouse and restimulated in vitro with control NP (−) or E7 peptide (±). The relative expression levels of IFN-γ mRNA were measured by real-time PCR and normalized to 18S rRNA levels. *B*, Eight-week-old C57BL/6 mice ($n = 10$) were inoculated subcutaneously with 1×10^5 TC-1 cells/mouse at 0 days and then immunized with control NP peptide (3 μg), E7 (3 μg), N′-CARD-PTD (5 μg), or E7 (3 μg) plus N′-CARD-PTD (5 μg) at 3, 4, 5, 6, and 7 days. Tumor sizes were measured at 14, 18, and 20 days. Data represent one of two independent experiments with similar results. *, $p < 0.01$.

N′-CARD-PTD augments Ag-specific acquired immune responses to protect against influenza virus infection and tumor outgrowth in vivo

To examine the in vivo effects of N′-CARD-PTD on innate and acquired immune responses, we used a mouse model of influenza virus infection and of tumor transplantation. Influenza split-product vaccine (flu vax) was used to evaluate the adjuvanticity of N′-CARD-PTD. Flu vax was prepared at The Research Foundation for Microbial Diseases of Osaka University from the purified influenza virus A/New Caledonia/20/99 strain treated sequentially with ether and formalin. As shown in Fig. 5*A*, s.c. administration of flu vax plus N′-CARD-PTD or CpG ODN induced significant levels of specific IgG1 production that were comparable to that of flu vax alone. Administration of flu vax plus N′-CARD-PTD or CpG ODN, by contrast, resulted in significantly higher levels of specific IgG2a production compared with that of flu vax alone, suggesting that N′-CARD-PTD and CpG ODN have the ability to modulate Th1-deviated immune responses. In accordance with such adjuvant effects, immunization with flu vax plus N′-CARD-PTD conferred superior protection against a lethal influenza challenge relative to that with flu vax alone (Fig. 5, *B* and *C*).

We next examined whether N′-CARD-PTD has an ability to enhance Ag-specific cellular immune responses. Immunization with MHC class I-restricted HPV E7 peptide (E7) alone induced minimal levels of E7-specific IFN-γ production from splenocytes (Fig. 6*A*). Treatment with E7 plus N′-CARD-PTD or CpG ODN induced higher levels of E7-specific IFN-γ production, suggesting that N′-CARD-PTD has an adjuvant effect on cell-mediated immune responses (Fig. 6*A*). Thus, mice were s.c. transplanted with TC-1 cells expressing E7 as a model tumor Ag, and then immunized with E7 in the presence or absence of N′-CARD-PTD, as shown in Fig. 6*B*. The outgrowth of TC-1 tumors in mice treated with either N′-CARD-PTD or E7 alone was comparable to that in mice treated with control NP peptide. In accordance with E7-specific IFN-γ production from splenocytes, the sizes of established tumors in mice treated with E7 plus N′-CARD-PTD were significantly smaller compared with those in mice treated with E7 alone or with N′-CARD-PTD alone (Fig. 6*B*). These in vivo results, taken together, indicate that N′-CARD-PTD, an activator of NDH-mediated innate immune responses, acts as a vaccine adjuvant, thereby enhancing protective immune responses against pathogens or tumors.

Discussion

This study provides the first evidence that the N′-CARD-PTD polypeptide directly enters the nucleus and triggers the innate immune signaling pathway leading to type I IFN production through NDH. NDH is a member of the DEXH (Asp-Glu-X-His) family of helicases and is highly conserved in higher eukaryotes, from *Drosophila* to mammals. Previous studies have shown that NDH interacts with molecules of the transcription machinery, such as the RNA polymerase II complex (28), cAMP-response element-binding protein (28), and NF-κB p65 (29), thereby regulating the transcription of responsive genes. NDH also acts together with the RNA editing enzyme to coordinate the editing and splicing of numerous cellular and viral RNAs (30, 31). Knockout of the *Ndh* gene led to early embryonic lethality (<E10.5) due to a high frequency of apoptosis in embryonic ectodermal cells during gastrulation (32). In addition to these properties of gene regulation and cellular homeostasis, our results suggest that NDH has a distinct property of mediating innate immune signaling upstream of TBK1. Recently, it was shown that a DEAD (Asp-Glu-Ala-Asp) box helicase, DDX3X, is a kinase substrate of TBK1 and acts as a critical component of TBK1-dependent innate immune signaling, particularly in the type I IFN production pathway (33).

MAPK activation plays a significant role in LPS- or CpG DNA-mediated signaling (Fig. 4*C* and Ref. 34), however, the signaling pathway induced by N′-CARD-PTD may not involve MAPK. This suggested that, unlike TLR-mediated signaling pathways, activation of MAPK is not crucial for N′-CARD-PTD-mediated type I IFN production. Rather, the action of N′-CARD-PTD resembles the signal activation induced by IFN stimulatory DNA, which was originally reported by Stetson et al. as having a similar action to B-DNA, which is critical in the control of DNA vaccine immunogenicity (5, 35). Because MAPK activation is associated with deleterious effects, ranging from hyperinflammation to cancer (36), the lack of such kinase activation would be an advantage for the repeated clinical application of N′-CARD-PTD. Further study will be needed to elucidate the molecular basis of the NDH-mediated signaling pathway and to determine the value of N′-CARD-PTD for clinical use.

Many TLR ligands and related compounds have been tested as vaccine adjuvants and as anti-allergy and anti-cancer drugs in humans (37). Among these, some clinical trials of TLR9-targeting molecules, including CpG ODN and its conjugated products, have recently been abandoned due to unexpectedly weaker responses in

humans relative to those observed in mice. This result was attributable to a lower frequency of TLR9 expression in human immune cells; expression was found in only a portion of B cells and plasmacytoid DCs that combined made up just 1% of the total immune cell population (38). In contrast, immunostimulatory RNA or B-DNA activates innate immune responses through cytosolic receptors but only when they are introduced into intracellular compartments, i.e., they have almost no effects when they are present outside the cell. Taking such observations into account, N′-CARD-PTD may have the advantage of self-transmigration into the nucleus and of triggering innate immune signaling in the absence of TLRs but in the presence of NDH and TBK1, which are ubiquitously expressed in a wide-variety of cell types.

In conclusion, this study showed concrete evidence that the activation of a distinct NDH-mediated signaling pathway up-regulates innate immune responses and that N′-CARD-PTD is a candidate vaccine adjuvant in future vaccine development. These findings may also provide insights that will be helpful in the design of immunomodulatory agents, such as using constitutively active signaling molecules of the innate immune responses.

Disclosures

The authors have no financial conflict of interest.

References

1. Barr, S. D., J. R. Smiley, and F. D. Bushman. 2008. The interferon response inhibits HIV particle production by induction of TRIM22. *PLoS Pathog.* 4: 1–11.
2. Fodil-Cornu, N., and S. M. Vidal. 2008. Type I interferon response to cytomegalovirus infection: the kick-start. *Cell Host Microbes* 3: 59–61.
3. Bracci, L., E. Proietti, and F. Belardelli. 2007. IFN-α and novel strategies of combination therapy for cancer. *Ann. NY Acad. Sci.* 1112: 256–268.
4. Ferrantini, M., I. Capone, and F. Belardelli. 2007. Interferon-α and cancer: mechanisms of action and new perspectives of clinical use. *Biochimie* 89: 884–893.
5. Ishii, K. J., T. Kawagoe, S. Koyama, K. Matsui, H. Kumar, T. Kawai, S. Uematsu, O. Takeuchi, F. Takeshita, C. Coban, and S. Akira. 2008. TANK-binding kinase-1 delineates innate and adaptive immune responses to DNA vaccines. *Nature* 451: 725–729.
6. Ishii, K. J., C. Coban, H. Kato, K. Takahashi, Y. Torii, F. Takeshita, H. Ludwig, G. Sutter, K. Suzuki, H. Hemmi, et al. 2006. A Toll-like receptor-independent antiviral response induced by double-stranded B-form DNA. *Nat. Immunol.* 7: 40–48.
7. Zhu, J., X. Huang, and Y. Yang. 2007. Innate immune response to adenoviral vectors is mediated by both Toll-like receptor-dependent and -independent pathways. *J. Virol.* 81: 3170–3180.
8. Takeuchi, O., and S. Akira. 2008. MDA5/RIG-I and virus recognition. *Curr. Opin. Immunol.* 20: 17–22.
9. Kawai, T., and S. Akira. 2007. Antiviral signaling through pattern recognition receptors. *J. Biochem.* 141: 137–145.
10. Yoshida, H., Y. Okabe, K. Kawane, H. Fukuyama, and S. Nagata. 2005. Lethal anemia caused by interferon-β produced in mouse embryos carrying undigested DNA. *Nat. Immunol.* 6: 49–56.
11. Kawane, K., M. Ohtani, K. Miwa, T. Kizawa, Y. Kanbara, Y. Yoshioka, H. Yoshikawa, and S. Nagata. 2006. Chronic polyarthritis caused by mammalian DNA that escapes from degradation in macrophages. *Nature* 443: 998–1002.
12. Kato, H., O. Takeuchi, S. Sato, M. Yoneyama, M. Yamamoto, K. Matsui, S. Uematsu, A. Jung, T. Kawai, K. J. Ishii, et al. 2006. Differential roles of MDA5 and RIG-I helicases in the recognition of RNA viruses. *Nature* 441: 101–105.
13. Cheng, G., J. Zhong, J. Chung, and F. V. Chisari. 2007. Double-stranded DNA and double-stranded RNA induce a common antiviral signaling pathway in human cells. *Proc. Natl. Acad. Sci. USA* 104: 9035–9040.
14. Takahasi, K., M. Yoneyama, T. Nishihori, R. Hirai, H. Kumeta, R. Narita, M. Gale, Jr., F. Inagaki, and T. Fujita. 2008. Nonself RNA-sensing mechanism of RIG-I helicase and activation of antiviral immune responses. *Mol. Cell* 29: 428–440.
15. Ishii, K. J., S. Koyama, A. Nakagawa, C. Coban, and S. Akira. 2008. Host innate immune receptors and beyond: making sense of microbial infections. *Cell Host Microbes* 3: 352–363.
16. Potter, J. A., R. E. Randall, and G. L. Taylor. 2008. Crystal structure of human IPS-1/MAVS/VISA/Cardif caspase activation recruitment domain. *BMC Struct. Biol.* 8: 11.
17. Loo, Y. M., D. M. Owen, K. Li, A. K. Erickson, C. L. Johnson, P. M. Fish, D. S. Carney, T. Wang, H. Ishida, M. Yoneyama, et al. 2006. Viral and therapeutic control of IFN-β promoter stimulator 1 during hepatitis C virus infection. *Proc. Natl. Acad. Sci. USA* 103: 6001–6006.
18. Sung, M., G. M. Poon, and J. Gariepy. 2006. The importance of valency in enhancing the import and cell routing potential of protein transduction domain-containing molecules. *Biochim. Biophys. Acta* 1758: 355–363.
19. Davenport, F. M., A. V. Hennessy, F. M. Brandon, R. G. Webster, C. D. Barrett, Jr., and G. O. Lease. 1964. Comparisons of serologic and febrile responses in humans to vaccination with influenza a viruses or their hemagglutinins. *J. Lab. Clin. Med.* 63: 5–13.
20. Tanimoto, T., R. Nakatsu, I. Fuke, T. Ishikawa, M. Ishibashi, K. Yamanishi, M. Takahashi, and S. Tamura. 2005. Estimation of the neuraminidase content of influenza viruses and split-product vaccines by immunochromatography. *Vaccine* 23: 4598–4609.
21. Kawai, T., K. Takahashi, S. Sato, C. Coban, H. Kumar, H. Kato, K. J. Ishii, O. Takeuchi, and S. Akira. 2005. IPS-1, an adaptor triggering RIG-I- and Mda5-mediated type I interferon induction. *Nat. Immunol.* 6: 981–988.
22. Jounai, N., F. Takeshita, K. Kobiyama, A. Sawano, A. Miyawaki, K. Q. Xin, K. J. Ishii, T. Kawai, S. Akira, K. Suzuki, and K. Okuda. 2007. The Atg5 Atg12 conjugate associates with innate antiviral immune responses. *Proc. Natl. Acad. Sci. USA* 104: 14050–14055.
23. Takeshita, F., K. Suzuki, S. Sasaki, N. Ishii, D. M. Klinman, and K. J. Ishii. 2004. Transcriptional regulation of the human TLR9 gene. *J. Immunol.* 173: 2552–2561.
24. Takeshita, F., K. J. Ishii, K. Kobiyama, Y. Kojima, C. Coban, S. Sasaki, N. Ishii, D. M. Klinman, K. Okuda, S. Akira, and K. Suzuki. 2005. TRAF4 acts as a silencer in TLR-mediated signaling through the association with TRAF6 and TRIF. *Eur. J. Immunol.* 35: 2477–2485.
25. Takeshita, F., T. Tanaka, T. Matsuda, M. Tozuka, K. Kobiyama, S. Saha, K. Matsui, K. J. Ishii, C. Coban, S. Akira, et al. 2006. Toll-like receptor adaptor molecules enhance DNA-raised adaptive immune responses against influenza and tumors through activation of innate immunity. *J. Virol.* 80: 6218–6224.
26. Seth, R. B., L. Sun, C. K. Ea, and Z. J. Chen. 2005. Identification and characterization of MAVS, a mitochondrial antiviral signaling protein that activates NF-κB and IRF 3. *Cell* 122: 669–682.
27. Fitzgerald, K. A., S. M. McWhirter, K. L. Faia, D. C. Rowe, E. Latz, D. T. Golenbock, A. J. Coyle, S. M. Liao, and T. Maniatis. 2003. IKKε and TBK1 are essential components of the IRF3 signaling pathway. *Nat. Immunol.* 4: 491–496.
28. Nakajima, T., C. Uchida, S. F. Anderson, C. G. Lee, J. Hurwitz, J. D. Parvin, and M. Montminy. 1997. RNA helicase A mediates association of CBP with RNA polymerase II. *Cell* 90: 1107–1112.
29. Tetsuka, T., H. Uranishi, T. Sanda, K. Asamitsu, J. P. Yang, F. Wong-Staal, and T. Okamoto. 2004. RNA helicase A interacts with nuclear factor κB p65 and functions as a transcriptional coactivator. *Eur. J. Biochem.* 271: 3741–3751.
30. Bratt, E., and M. Ohman. 2003. Coordination of editing and splicing of glutamate receptor pre-mRNA. *RNA* 9: 309–318.
31. Maas, S., A. Rich, and K. Nishikura. 2003. A-to-I RNA editing: recent news and residual mysteries. *J. Biol. Chem.* 278: 1391–1394.
32. Lee, C. G., V. da Costa Soares, C. Newberger, K. Manova, E. Lacy, and J. Hurwitz. 1998. RNA helicase A is essential for normal gastrulation. *Proc. Natl. Acad. Sci. USA* 95: 13709–13713.
33. Soulat, D., T. Burckstummer, S. Westermayer, A. Goncalves, A. Bauch, A. Stefanovic, O. Hantschel, K. L. Bennett, T. Decker, and G. Superti-Furga. 2008. The DEAD-box helicase DDX3X is a critical component of the TANK-binding kinase 1-dependent innate immune response. *EMBO J.* 27: 2135–2146.
34. Hacker, H., H. Mischak, G. Hacker, S. Eser, N. Prenzel, A. Ullrich, and H. Wagner. 1999. Cell type-specific activation of mitogen-activated protein kinases by CpG-DNA controls interleukin-12 release from antigen-presenting cells. *EMBO J.* 18: 6973–6982.
35. Stetson, D. B., and R. Medzhitov. 2006. Recognition of cytosolic DNA activates an IRF3-dependent innate immune response. *Immunity* 24: 93–103.
36. Salh, B. 2007. c-Jun N-terminal kinases as potential therapeutic targets. *Expert Opin. Ther. Targets.* 11: 1339–1353.
37. Kanzler, H., F. J. Barrat, E. M. Hessel, and R. L. Coffman. 2007. Therapeutic targeting of innate immunity with Toll-like receptor agonists and antagonists. *Nat. Med.* 13: 552–559.
38. Schmidt, C. 2007. Clinical setbacks for Toll-like receptor 9 agonists in cancer. *Nat. Biotechnol.* 25: 825–826.

Analytical Biochemistry 387 (2009) 60–63

Contents lists available at ScienceDirect

Analytical Biochemistry

journal homepage: www.elsevier.com/locate/yabio

Isoelectric focusing of high-molecular-weight protein complex under native conditions using agarose gel

Ryo Yokoyama, Yuko Iwafune, Hiroshi Kawasaki *, Hisashi Hirano

Supramolecular Biology, International Graduate School of Arts and Sciences, Yokohama City University, Suehiro-cho 1-7-29, Tsurumi-ku, Yokohama 230-0045, Japan

ARTICLE INFO

Article history:
Received 18 September 2008
Available online 15 January 2009

Keywords:
Isoelectric focusing
Protein complex
Yeast

ABSTRACT

The isolation and characterization of protein complexes are essential steps toward understanding cellular functions. A method for separating and characterizing high-molecular-weight protein complexes using two-dimensional polyacrylamide gel electrophoresis (2D-PAGE) with native agarose gel isoelectric focusing (IEF) is described. Using this method, fractions containing high-molecular-weight protein complexes were analyzed. The advantages of using native agarose gel IEF include the ability to concentrate the protein complexes and the ease of handling when performing 2D separations. Although limited with respect to the size of molecules and particles that may be separated, this method is useful for the isolation and characterization of high-molecular-weight protein complexes.

Proteins are functional elements of a cell, and reversible protein–protein interactions are characteristic of most biochemical pathways. However, a cell is not a complex mixture of proteins and other molecules randomly colliding with each other. Biochemical reactions in a cell are organized and sophisticated. Every major cellular process is carried out by protein complexes, or molecular machines, such as the ribosome and proteasome [1]. The isolation and characterization of protein complexes are essential steps toward understanding cellular functions [2–4]. Affinity purification has been used recently to purify protein complexes [5]. Among these methods, tandem affinity purification (TAP)[1] is known as the most powerful purification tool and is used to purify protein complexes under mild conditions based on affinity for protein A and a calmodulin-binding peptide in the TAP tag. By combining affinity purification with mass spectrometry (MS), we can identify the components of a protein complex to elucidate the protein interaction network [6,7]. However, some proteins in an isolated complex may interact indirectly with each other, or the affinity-tagged protein may be involved in multiple complexes. Ideally, an isolated protein complex should be separated further to allow a detailed investigation of its composition [8,9]. Another shortcoming of affinity or conventional purification methods is that the purified proteins are usually diluted. Separation, purification, and characterization of high-molecular-weight protein complexes are usually performed using ultracentrifugation, gel partition chromatography, and electrophoresis. These methods are difficult to apply to diluted samples. Alternatively, isoelectric focusing (IEF) can be used to separate and concentrate protein complexes under mild conditions without destroying the complex [10]. IEF without denaturing reagents such as urea and detergents has been used for the separation of serum proteins and cytosolic proteins [11]. There have been few reports of IEF on the separation of high-molecular-weight complex under native conditions. IEF is possible without matrix such as polyacrylamide gels, but the focusing ability is usually sacrificed by recovery of separated proteins into multichamber, for example. Acrylamide gels have limitations to focus higher molecular weight proteins in the case of denatured protein separation, and agarose gel is suitable to separate higher molecular weight proteins under denatured conditions [12,13].

Here we describe a method for the separation and characterization of high-molecular-weight protein complexes by IEF using agarose gel. This method was applied to separate and analyze high-molecular-weight protein complexes in fractions isolated from yeast.

Materials and methods

Materials

Yeast strain B-8032 (*MATa ura3-52 CYC1-963 cyc7-67 lys5-10*) was used. L-1-*p*-Tosylamino-2-phenylethyl chloromethyl ketone (TPCK)–trypsin was obtained from Sigma (St. Louis, MO, USA). 4-Methylcoumaryl-7-amide (MCA) substrates were obtained from

* Corresponding author. Fax: +81 45 508 7667.
E-mail address: kawasaki@yokohama-cu.ac.jp (H. Kawasaki).

[1] *Abbreviations used:* TAP, tandem affinity purification; MS, mass spectrometry; IEF, isoelectric focusing; TPCK, L-1-*p*-tosylamino-2-phenylethyl chloromethyl ketone; MCA, 4-methylcoumaryl-7-amide; EDTA, ethylenediaminetetraacetic acid; SDS-PAGE, sodium dodecyl sulfate-polyacrylamide gel electrophoresis; BIS, *N,N'*-methylene-bis-acrylamide; TFA, trifluoroacetic acid; MALDI-TOF MS, matrix-assisted laser desorption/ionization time-of-flight mass spectrometry; DTT, dithiothreitol; 2D, two-dimensional.

0003-2697/$ - see front matter © 2009 Elsevier Inc. All rights reserved.
doi:10.1016/j.ab.2009.01.009

the Peptide Institute (Osaka, Japan). α-Cyano-4-hydroxy-cinnamic acid was purchased from Aldrich (Milwaukee, WI, USA). Protease inhibitor cocktail (Complete, ethylenediaminetetraacetic acid [EDTA] free) was supplied by Roche Diagnostics K.K. (Tokyo, Japan).

Native IEF using agarose gels

Native IEF was performed in an agarose tube gel without the addition of denaturing reagents such as urea and detergent. Gels were prepared from an agarose solution prepared by mixing 30 mg of agarose IEF (GE Healthcare, Buckinghamshire, UK) and 0.3 g of sorbitol in 2.7 ml of distilled water and heating in a microwave until dissolved. After cooling to approximately 40 °C, 300 μl of carrier ampholite (ampholine pH 3.5–10.0) was added and mixed. The agarose tube gel was prepared by drawing the agarose solution into a glass tube using a syringe connected via rubber tubing. IEF separation was carried out with 40 mM NaOH as the anode solution and 40 mM phosphoric acid as the cathode solution and using 80, 160, and 320 V for 30 or 40 min each.

SDS–PAGE

Proteins separated by native IEF were further separated by using sodium dodecyl sulfate–polyacrylamide gel electrophoresis (SDS–PAGE) according to the method of Laemmli [14] or according to the procedure described by Hirano, which uses a low BIS (*N,N'*-methylene-bis-acrylamide) polyacrylamide gel [15].

In-gel digestion and peptide mass fingerprinting using MALDI–TOF MS

A protein band was excised from the SDS–PAGE gel and cut into small pieces, which were incubated in a solution containing 50% (v/v) acetonitrile, 0.1% (v/v) trifluoroacetic acid (TFA), and 0.5% (v/v) *N*-ethylmorpholine for 1 h at 37 °C to remove the protein stain. The gel pieces were washed with water, and then 5 μl of 0.3 M *N*-ethylmorpholine/acetate (pH 8.2) and 1 μl of 140 mM 2-mercaptoethanol were added. After a 30-min incubation at 37 °C, 1 μl of TPCK–trypsin (50 μg/ml) was added to digest the protein at 37 °C for 16 h. Peptide mass fingerprinting was performed using matrix-assisted laser desorption/ionization time-of-flight mass spectrometry (MALDI–TOF MS, Tof Spec 2E, Micromass, Manchester, UK) and a matrix solution of 60% (v/v) acetonitrile saturated with α-cyano-4-hydroxy-*trans*-cinnamic acid. The peptides produced by the in-gel digestion were concentrated using a ZipTip C_{18} (Millipore, Billerica, MA, USA), and the samples were prepared by mixing 1 μl of peptides and 1 μl of matrix solution on a target plate. Proteins were identified by using ProteinLynx Global Server (search parameters used: database, Swiss–Prot (yeast); enzyme, trypsin; modification, methionine oxidation and/or cysteine propionamide; missed cleavage, 1; mass tolerance, 0.15 Da). Top-ranked protein with at least three peptide matches by the search was listed as identified.

Separation of high-molecular-weight protein complexes extracted from yeast cells

Yeast cells were grown in YPD medium (10 g of yeast extract, 20 g of bactopeptone, and 20 g of glucose per liter) at 29 °C for 72 h with continuous shaking at 160 rpm and then were harvested by centrifugation at 2000 *g* for 10 min. Cell extracts were prepared by vortexing a suspension of cells (~60 g of yeast, 50% [v/v]) with 0.45-mm glass beads in buffer A (50 mM Tris–HCl [pH 7.5] containing 10% [v/v] glycerol, 1 mM dithiothreitol [DTT], and protease inhibitor cocktail) on ice. The beads and unbroken cells were removed by centrifugation at 8000 rpm for 20 min (Beckman Rotor JLA-10.500). Microsomes and organelles were removed by three successive centrifugation steps: 15,000 rpm for 30 min (Beckman Rotor JA-25.50), 17,000 rpm for 40 min (Beckman Rotor JA-25.50), and 60,000 *g* for 60 min. The high-molecular-weight proteins were precipitated by ultracentrifugation at 265,000 *g* for 5 h, and the precipitate was dissolved in 80 ml of buffer A. Materials that did not dissolve were removed by centrifugation at 12,000 rpm for 20 min (Beckman Rotor JA-25.50). The high-molecular-weight proteins were again precipitated by ultracentrifugation at 265,000 *g* for 5 h, the precipitate was dissolved in 7 ml of buffer A, and the undissolved materials were removed by centrifugation at 8000 rpm for 25 min (Beckman Rotor JA-20.50). Approximately 600 mg of protein was recovered. The proteins in 3 ml of the recovered protein solution were separated by gel chromatography using a Bio-Gel A 1.5-m column (2.5 [i.d.] × 45 cm) at a flow rate of 0.3 ml/min, and 3-ml fractions were collected. The fractions containing protein complexes slightly smaller than the 20S proteasome were pooled, and the proteins were separated by anion exchange chromatography using a Poros HQ/20 column with a linear gradient of KCl in 25 mM Tris–HCl (pH 7.5) at a flow rate of 5 ml/min. Protein complexes were recovered in six fractions. Each fraction was desalted with a CentriPlus 30 filter and further separated by ultracentrifugation through a glycerol density gradient at 28,000 rpm for 23 h (SW28 rotor). The proteins in each fraction were analyzed by SDS–PAGE or two-dimensional (2D)–PAGE with IEF in native agarose gels.

Results and discussion

Separation of proteasome complexes by native IEF

Proteasomes are multisubunit complexes that degrade ubiquitinated proteins. The 20S proteasome consists of a stack of four rings, each of which is composed of seven α or β subunits [16]. The 20S proteasome is cylindrical, with a molecular weight of approximately 700 kDa. In the current study, the 20S proteasome was purified from yeast cells. Fig. 1 shows the electrophoretic separation of the 20S proteasome using SDS–PAGE and native IEF–PAGE. The subunits of 20S proteasome were separated by SDS–PAGE (Fig. 1A). The 20S proteasome was well focused by native IEF in an agarose gel. All subunits were focused at the same p*I* by the native IEF (Fig. 1B). Under denatured conditions, the subunits of 20S proteasome were usually separated with their p*I* by IEF [17]. The proteins from a crude fraction containing the 20S

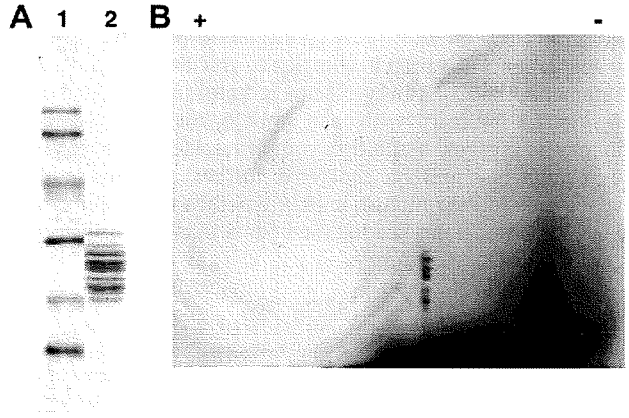

Fig. 1. Separation of proteasomes. (A) Separation of proteasome subunits by SDS–PAGE. Lane 1: molecular weight markers (from the upper band, 94, 67, 43, 30, 20, and 14 kDa); lane 2: 20S proteasome subunits. (B) Separation of proteasome subunits by 2D–PAGE with native IEF. The 20S proteasome complex was focused by native IEF, and the proteasome subunits were separated by SDS–PAGE (second dimension).